Transportation Research Part B xxx (xxxx) xxx

Contents lists available at ScienceDirect

Transportation Research Part B

journal homepage: www.elsevier.com/locate/trb

H_∞ robust perimeter flow control in urban networks with partial information feedback

Reza Mohajerpoor[a,b,*], Meead Saberi[c], Hai L. Vu[d], Timothy M. Garoni[e], Mohsen Ramezani[a,*]

[a] The University of Sydney, School of Civil Engineering, Sydney, Australia
[b] Data61, CSIRO, Sydney, Australia
[c] School of Civil and Environmental Engineering, University of New South Wales, Sydney, Australia
[d] Institute of Transport Studies, Department of Civil Engineering, Monash University, Clayton, VIC 3800, Australia
[e] ARC Centre of Excellence for Mathematical and Statistical Frontiers (ACEMS), School of Mathematical Sciences, Monash University, Clayton, Victoria 3800, Australia

ARTICLE INFO

Article history:
Received 16 September 2018
Revised 11 March 2019
Accepted 12 March 2019
Available online xxx

Keywords:
Network fundamental diagram
Gating
Observer based control
Robust H-infinity control
Traffic flow

ABSTRACT

Perimeter control is an effective city-scale solution to tackle congestion problems in urban networks. To accommodate the unpredictable dynamics of congestion propagation, it is essential to incorporate real-time robustness against travel demand fluctuations into a pragmatic perimeter control strategy. This paper proposes robust perimeter control algorithms based on partial information feedback from the network. The network dynamics are modeled using the concept of the Macroscopic Fundamental Diagram (MFD), where a heterogeneously congested network is assumed to be partitioned into two homogeneously congested regions, and an outer region that acts as demand origin and destination. The desired operating condition of the network is obtained by solving an optimization program. Observer-based H_∞ proportional (P) and proportional-integral (PI) controllers are designed based on Lyapunov theory, to robustly regulate the accumulation of each region and consequently to maximize the network outflow. The controller design algorithms further accommodate operational constraints by guarantying: (i) the boundedness of the perimeter control signals and (ii) a bounded offset between the perimeter control signals. Control parameters are designed off-line by solving a set of linear matrix inequalities (LMI), which can be solved efficiently. Comprehensive numerical studies conducted on the nonlinear model of the network highlight the effectiveness of the proposed robust control algorithms in improving the congestion in the presence of time-varying disturbance in travel demand.

1. Introduction

Congestion in cities is rapidly increasing due to population growth and the limited capacity of road networks. Among the remedies to this rising problem are: (i) infrastructure construction, (ii) congestion pricing, and (iii) improving the efficiency of traffic control strategies. Solution (i) is extremely costly and solution (ii) despite sound theoretical support is still hindered by political barriers. On the other hand, solution (iii) could potentially provide cost effective and sustainable resolutions that can be implemented in conjunction with the other methods to alleviate congestion.

* Corresponding authors.
E-mail addresses: reza.mohajerpoor@csiro.au (R. Mohajerpoor), mohsen.ramezani@sydney.edu.au (M. Ramezani).

https://doi.org/10.1016/j.trb.2019.03.010
0191-2615/

The most common method of traffic control in urban networks is through traffic signals. However, controlling multiple traffic signals in a complex and large urban network in a centralized manner is challenging both mathematically and computationally. This is due to several complexities such as uncertainties in travel demand, lack of real-time measurements of traffic flows and queue lengths at every intersection, as well as the curse of dimensionality stemming from the size of the problem increasing with the number of controlled intersections. Modeling the traffic dynamics of networks at the macroscopic scale provides an opportunity to reduce the complexity of the microscopic interactions. This is achievable using the concept of the Network Macroscopic Fundamental Diagram (MFD or NFD) Daganzo (2007); Geroliminis and Daganzo (2008), which relates the rate that vehicles inside the network finish their trips to their accumulation.

The outflow-accumulation MFD, in conjunction with the conservation of flows principle, can be used to derive an accumulation-based macroscopic dynamic model of a single traffic network or multiple traffic subnetworks Geroliminis et al. (2013); Mahmassani et al. (2013); Kouvelas et al. (2017); Haddad and Mirkin (2017). The speed-accumulation MFD can be further used to develop event-based modeling of trip duration and congestion level Mariotte et al. (2017). The accumulation-based dynamic model can be used to control the inflow and outflow of the regions by controlling the traffic signals on each region's perimeter, with the objective of regulating the accumulation of vehicles inside the region in real-time Geroliminis et al. (2013). This city-level control scheme, i.e. perimeter flow control, has been studied in the literature, from different perspectives Geroliminis et al. (2013); Keyvan-Ekbatani et al. (2012); Ramezani et al. (2015). An MFD further enables investigation of congestion pricing Liu and Geroliminis (2017); Gu et al. (2018), region-based routing Yildirimoglu et al. (2015); Leclercq et al. (2015); Yildirimoglu et al. (2018), large-scale analyses of multi-modal networks, e.g. Ramezani and Nourinejad (2018); Amirgholy and Gonzales (2016); Loder et al. (2017); Chiabaut et al. (2018), and network-wide demand management Yildirimoglu and Ramezani (2019). Moreover, MFD estimation has been studied in e.g. Leclercq et al. (2014); Laval and Castrillón (2015).

Part of the MFD-based network perimeter control literature focuses on nonlinear control algorithms such as model predictive control (MPC), which generally require real-time network state variables and prediction of demand (see e.g. Geroliminis et al. (2013); Ramezani et al. (2015); Yang et al. (2018)). Although MPC algorithms have shown promising performance when applied to single and multi-region networks (e.g. Ramezani et al. (2015)), their implementation is often computationally expensive (depending on the prediction time horizon) compared to classical feedback regulators such as proportional-integral-derivative (PID) controllers. In addition, MPC robustness to accommodate model uncertainties and unpredicted demand disturbances needs careful attention.

Linear control techniques such as PID and adaptive control algorithms on the other hand, provide cost effective and pragmatic solutions that can handle parametric uncertainties and bounded disturbance effects Aboudolas and Geroliminis (2013); Kouvelas et al. (2017); Haddad and Mirkin (2017). Kouvelas et al. Kouvelas et al. (2017) employ a dynamic MFD model of the network by neglecting the internal dynamics (as in Aboudolas and Geroliminis (2013)) and design a proportional-integral (PI) controller using an adaptive fine-tuning algorithm based on heuristic techniques. Haddad and Mirkin in Haddad and Mirkin (2016, 2017) propose adaptive control algorithms that guarantee the asymptotic stability of the controlled networks in the presence of the system's parametric uncertainties and disturbances. However, the proposed methods neglect inherent bounds on the perimeter control signals in the controller design process. Very recently, Zhong et al. Zhong et al. (2018a) proposed nonlinear control algorithms for robust perimeter control of a two-region traffic network based on the Lyapunov theory. They extended the proposed algorithm to a multi-region network in Zhong et al. (2018b).

A few existing algorithms consider the real-time variation of demand from the nominal values (e.g. Haddad and Mirkin (2017, 2016); Ampountolas et al. (2017); Zhong et al. (2018a,b)) in the controller design process. This is crucial as demand disturbances (as in Kouvelas et al. (2017); Geroliminis et al. (2013); Aboudolas and Geroliminis (2013); Keyvan-Ekbatani et al. (2015)) may result in degraded performance of the closed-loop controlled system. H_∞ control synthesis Doyle et al. (1989); Gahinet and Apkarian (1994) provides an effective method for designing control algorithms for linear or nonlinear systems, to ensure the stability of the system in the presence of bounded disturbances. This method has been applied to robust ramp metering of freeways Lemarchand et al. (2011). However, H_∞ control has not yet been considered for the perimeter control of MFD-based traffic models. Moreover, the literature has generally assumed that the traffic state information is fully observable Geroliminis et al. (2013); Kouvelas et al. (2017); Haddad and Mirkin (2017); Keyvan-Ekbatani et al. (2012); Ramezani et al. (2015). This includes accumulation of vehicles in the network, together with the number of vehicles that aim to finish their travel within the network or have a destination outside the network. However, real-time collection of the data related to the destination of each traveller is difficult and may not be feasible in the foreseeable future. Additionally, the majority of the literature assumes uncorrelated perimeter control values for the inbound and outbound travel directions. Although, this strategy results in more degrees of freedom (DoFs) for the controller, it may result in impractical signal timing at the controlled intersections Luk and Green (2010). For instance, it is possible that we attain $u_{21} = 0.2$ for the high demand direction and $u_{12} = 0.9$ for the opposite direction, to maintain the accumulation of the inner Region 1 at a desired level (see Fig. 1). Note that u_{ij} is the gated transfer flow to demand ratio from Region i to Region j, $i, j = \{1, 2\}$ (see the nomenclature below). Therefore, as a consequence of gating for an intersection that connects Region 2 to Region 1, we might allocate 90% of the green time to the less congested direction (movement towards Region 2), while only 20% of the green time is allocated to the opposite direction (movement towards Region 1) that is heavily congested.

Motivated by the above, we propose effective robust control algorithms to address the above problems for a network partitioned into two homogeneous regions (subnetworks) with two controlled perimeters. To this end, optimal permissible setpoint accumulations and Steady-State (SS) control signals are computed by solving an optimization problem, given the nomi-

Please cite this article as: R. Mohajerpoor, M. Saberi and H.L. Vu et al., H_∞ robust perimeter flow control in urban networks with partial information feedback, Transportation Research Part B, https://doi.org/10.1016/j.trb.2019.03.010

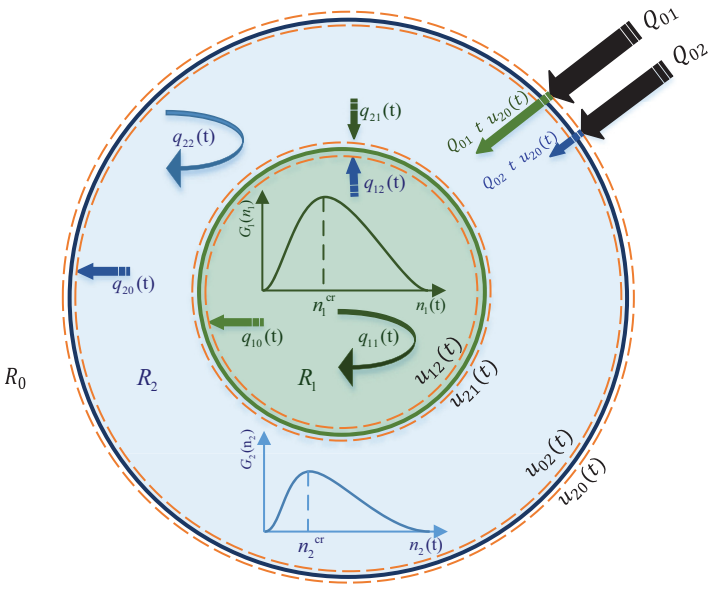

Fig. 1. The schematic diagram of the network representing the MFDs, control signals, and demand generated within the regions, or transferred between the regions. Demand generated from the outer region R_0 is gated at Perimeter 2, in a way that flow $Q_{02}u_{02}$ is added to the traffic in R_2 with destination in R_2 (i.e. n_{22}), and flow $Q_{01}u_{02}$ is added to the traffic in R_2 who aim to finish their travel in R_1 (i.e. n_{21}). Note that the accumulation of the outer region R_0 is neither modelled nor controlled.

nal demand during the demand peak period. Furthermore, we develop observer-based robust H_∞ linear control strategies for the linearized model of the network based on Lyapunov theory, which is an energy based method (see Doyle et al. (1989); Gahinet and Apkarian (1994); Khalil and Grizzle (2002) for more information on Lyapunov theory and H_∞ robust control, and Mohajerpoor et al. (2015a,b) for more information on observer design). Proportional (P) and proportional-integral (PI) control architectures are separately designed, and their stability conditions are expressed in terms of Linear Matrix Inequalities (LMIs), which can be efficiently solved by any convex optimization algorithm Boyd et al. (1994). The controllers account for bounded variations of demand from the nominal value, and guarantee the boundedness of the control actions. Moreover, the design algorithms ensure the difference of control signals on each perimeter remains within a given threshold. A pseudo bang-bang control scheme is further proposed mainly for benchmarking purposes. We provide results of numerical experiments to elaborate the controller design procedure and highlight the effectiveness of the proposed control algorithms. Given the nonlinear nature of the network, the controllers' robust performance in efficiently regulating the accumulation of each region is emphasized.

In summary, the contributions of the paper are as follows:

- Admissible set-point accumulations and set-point control signals are obtained off-line from an optimization problem.
- The controllers are designed based on the Lyapunov theory to guarantee the asymptotic stability and robust performance of the linearized model in the presence of bounded demand disturbances. Control parameters are obtained off-line from solving a convex LMI program, which can be efficiently solved (computational complexity is polynomial time Boyd et al. (1994)).
- Employing the observer in the control structure, the controller only intakes partial information feedback from the network, instead of the full state measurements. This mitigates the existing barriers in real-time collection of data related to the destination of travellers.
- The controller design algorithm limits the perimeter control signals of the linearized model within the minimum and maximum values. The controller design algorithm further guarantees a bounded offset between the control signals of the inbound and outbound directions.

The rest of the paper is organized as follows. Nonlinear dynamics of the network and the linearization of the model are introduced in Section 2. Section 3 presents the proposed robust control algorithms. Illustrative numerical experiments are given in Section 4, and a summary and discussion of future direction are given in Section 5.

2. Dynamic modelling of the network

2.1. Preliminaries

Notations: Throughout the paper, $\mathbb{R}^m$ denotes the vector space of real m-tuples; $\mathbb{R}^{m\times p}$ the space of $m\times p$ real matrices; $\mathbb{S}^{m\times m}$ the space of $m\times m$ real symmetric matrices; I_m the $m\times m$ identity matrix; $\mathbf{0}$ the zero matrix with appropriate

Please cite this article as: R. Mohajerpoor, M. Saberi and H.L. Vu et al., H_∞ robust perimeter flow control in urban networks with partial information feedback, Transportation Research Part B, https://doi.org/10.1016/j.trb.2019.03.010

dimension; $\mathrm{He}(X) = X + X^T$ for a square matrix X and X^{-1} denotes its inverse; $\mathrm{diag}(X_1, \cdots, X_m)$ indicates a block diagonal matrix with matrices X_1 to X_m on the diagonal; $\|x\|$ is the Euclidean norm of vector x; $\mathbf{e}_\nu$ is a row vector with appropriate dimension with element number $\nu \geq 1$ equal to 1 and all the other elements of 0; $X_{(\nu)}$ indicates the row number ν of array X (i.e. $X_{(\nu)} = \mathbf{e}_\nu X$); and $\|X\|_F$ is the Frobenius norm of matrix X. Moreover, $M \succ 0$ ($\prec 0$) and $M \succeq 0$ ($\preceq 0$) indicate that square matrix M is positive (negative) definite and positive (negative) semi-definite, respectively.

Nomenclature

$n_i(t)$	Accumulation of Region i at time t, [veh]
n_i^{j}	Jam accumulation of Region i, [veh]
n_i^{cr}	Critical accumulation of Region i, where the maximum outflow occurs, [veh]
n_i^*	Steady-state (or equilibrium) accumulation of Region i, [veh]
$n_{ij}(t)$	Number of vehicles in Region i with destinations in Region j at time t, [veh]
$G_i(n_i(t))$	Outflow of Region i, [veh/s]
$Q_{0i}(t)$	Controllable demand from the outer Region 0 to Region i, [veh/s]
$u_{ij}(t)$	Transfer demand flow split from Region i to Region j that is allowed to cross the perimeter, that is the perimeter control signal at time t
$q_{ij}(t)$	Demand generated in Region i with destination in Region j at time t, [veh/s]
δ_i	Prescribed difference between the inbound and outbound perimeter control signals on Perimeter $i = \{1, 2\}$
Ω_n	Set {1, 2, 11, 22, 10, 20} as indices for the elements of the state vector
Ω_u	Set {12, 21, 02, 20} as indices for the elements of the control vector
Ω_r	Set {0, 1, 2} as indices for the regions

In this paper, without loss of generality, and for the sake of simplicity, the traffic network is assumed to be partitioned into three regions. Based on this assumption, our network comprises two regions, each represented by a well-defined MFD, and an outer region, 0, which generates controllable demand to Region 2 that includes vehicles with destinations in Regions 1 and 2 (i.e. $Q_{0i}(t)$, $i = \{1, 2\}$). Regulating the accumulation of Region 0 is not of interest, as we assume it comprises suburban areas and pertains a large capacity to store vehicles, thus it less likely gets congested. Therefore, vehicle accumulation and traffic dynamics of Region 0 are not incorporated into the model.

A schematic diagram of the inner and outer regions, their MFDs, perimeter control locations, and demand flows are depicted in Fig. 1. Note that in this paper, the perimeter control also regulates the transfer flow over the outer boundary between Regions 2 and 0. This has not been considered in the majority of papers on network perimeter control, see e.g. Geroliminis et al. (2013); Kouvelas et al. (2017); Haddad and Mirkin (2017) among others.

The number of vehicles in each region can be expressed as the sum of the number of vehicles moving towards a destination inside the region and the number of vehicles moving towards a destination outside the region:

$$n_1(t) = n_{11}(t) + n_{12}(t) + n_{10}(t), \tag{1a}$$

$$n_2(t) = n_{22}(t) + n_{21}(t) + n_{20}(t), \tag{1b}$$

where n_i, $i = \{1, 2\}$, is the accumulation of Region i, and n_{ij} is the number of vehicles in Region i with destinations in Region $j \in \Omega_r = \{0, 1, 2\}$.

The aim of the controller is to adjust the proportions of the flows permitted to travel between the regions (i.e. $u_{12}(\cdot)$, $u_{21}(\cdot)$, $u_{02}(\cdot)$, and $u_{20}(\cdot)$) using a robust feedback regulator. Moreover, there must be a lower-limit and an upper-limit for the control signal $u_k(t)$, $k \in \Omega_u = \{12, 21, 02, 20\}$, to realize the minimum and maximum green to cycle time ratios of the intersections that are controlled by the perimeter control strategy:

$$\begin{aligned} &0 < u_1^{\min} \leq u_i(t) \leq u_1^{\max} < 1 \qquad i = \{12, 21\}, \\ &0 < u_2^{\min} \leq u_j(t) \leq u_2^{\max} < 1 \qquad j = \{02, 20\}. \end{aligned} \tag{2}$$

Conditions in (2) imply the general operational constraints on the signal timing of the controlled intersections on each perimeter. For instance, a control signal cannot be equal to one, since under a high inter-region demand the full cycle length of each controlled intersection on the perimeter should be devoted to the green time of the phase serving vehicles moving towards a region. This will result in the full blockage of the other conflicting movements at the intersection, which is not feasible.

Furthermore, most of the existing perimeter control algorithms assume uncorrelated perimeter control values (i.e. green times) for the inbound and outbound movements. This assumption provides more DoF for the control algorithm in achieving the controller objectives. However, this might not be implementable in practice, because the green times for opposite flow directions (enforced by pairs ($u_{12}(t)$, $u_{21}(t)$) and ($u_{02}(t)$, $u_{20}(t)$)) might belong to the same phase, and hence be correlated. Accordingly, we relax this assumption in this paper, and consider that the difference between perimeter control values of the inbound and outbound directions is bounded. These constraints on the perimeter control signals read as:

$$\begin{aligned} &-\delta_1 \leq u_{21}(t) - u_{12}(t) \leq \delta_1, \\ &-\delta_2 \leq u_{20}(t) - u_{02}(t) \leq \delta_2, \end{aligned} \tag{3}$$

where $0 \leq \delta_i < 1$, $i = \{1, 2\}$, is the upper-bound of the allowed difference between the inbound and outbound perimeter control values of perimeter i. As a special case, $\delta_i = 0$ implies equal gated proportions of demand crossing perimeter i.

Please cite this article as: R. Mohajerpoor, M. Saberi and H.L. Vu et al., H_∞ robust perimeter flow control in urban networks with partial information feedback, Transportation Research Part B, https://doi.org/10.1016/j.trb.2019.03.010

2.2. Nonlinear dynamics of the network

The following assumptions are used in deriving the mathematical model of the network: [A] vehicles with internal trips in a region do not cross the perimeters, [B] trip lengths of vehicles within a region with internal or external destinations are similar and time-invariant, [C] the internal (external) trip completion rate in each region is proportional to the accumulation of vehicles in the region with internal (external) destinations Geroliminis et al. (2013), and [D] the receiving capacity of each region is not incorporated into the model. Considering the conservation of flows principle, together with Assumptions [A-D], the equations below describe the nonlinear model of traffic propagation in the network:

$$\dot{n}_{11}(t) = -\frac{n_{11}(t)}{n_1(t)}G_1(n_1(t)) + \frac{n_{21}(t)}{n_2(t)}G_2(n_2(t))u_{21}(t) + q_{11}(t), \tag{4a}$$

$$\dot{n}_{22}(t) = -\frac{n_{22}(t)}{n_2(t)}G_2(n_2(t)) + \frac{n_{12}(t)}{n_1(t)}G_1(n_1(t))u_{12}(t) + Q_{02}(t)u_{02}(t) + q_{22}(t), \tag{4b}$$

$$\dot{n}_{12}(t) = -\frac{n_{12}(t)}{n_1(t)}G_1(n_1(t))u_{12}(t) + q_{12}(t), \tag{4c}$$

$$\dot{n}_{21}(t) = -\frac{n_{21}(t)}{n_2(t)}G_2(n_2(t))u_{21}(t) + Q_{01}(t)u_{02}(t) + q_{21}(t), \tag{4d}$$

$$\dot{n}_{10}(t) = -\frac{n_{10}(t)}{n_1(t)}G_1(n_1(t))u_{12}(t) + q_{10}(t), \tag{4e}$$

$$\dot{n}_{20}(t) = -\frac{n_{20}(t)}{n_2(t)}G_2(n_2(t))u_{20}(t) + \frac{n_{10}(t)}{n_1(t)}G_1(n_1(t))u_{12}(t) + q_{20}(t), \tag{4f}$$

where $G_i(n_i(t))$ is the outflow of Region $i \in \{1, 2\}$ at time t with accumulation $n_i(t)$, given by the MFD. Q_{0i} is the controllable exogenous demand (passing through controlled intersections) from outer Region 0 to Region 2 with destination in Region i, and q_{ij} is the exogenous (uncontrollable) demand from Region $i \in \{1, 2\}$ with destination in Region $j \in \Omega_r$.

Assumptions [A-D] are the principal assumptions used to derive the dynamic model (4). They have been used in the majority of previous studies on the control of MFD-based traffic networks (see e.g. Geroliminis et al. (2013); Keyvan-Ekbatani et al. (2012); Kouvelas et al. (2017); Haddad and Mirkin (2017); Ramezani et al. (2015)), and they have been discussed in Daganzo (2007); Geroliminis and Daganzo (2008); Ramezani et al. (2015). Assumption [A] ensures that the outflow of a region corresponding to the external trips does not contain the flow of vehicles with internal destinations. Otherwise, there would be a portion of flow $n_{ii}/n_iG_i(n_i)$ travelling to the other region adding to n_{ji}, ($i \in \{1, 2\}$, $j \in \Omega_r$, and $i \neq j$) Yildirimoglu et al. (2015). Assumption [B] can be readily relaxed by considering a production-MFD and its relation to outflow-MFD. This has been studied in Ramezani et al. (2015) among others. Assumption [C] relates the region's outflow to the ratios between the accumulations based on the destination, which holds in steady-state conditions (Little's law). Moreover, Assumption [D] ensures that there is enough receiving capacity in a region for the demand flow that is transferred from the other regions. Otherwise, if for example Region 1 does not possess enough receiving capacity for the transfer flow demand from Region 2, due to e.g. the congestion of downstream links, then only a portion of the demand can be transferred, violating model (4). This is a not a limiting modeling assumption when a proper perimeter controller is applied as the controller should avoid the gridlock of the regions. A detailed modeling approach to address the receiving capacity for smaller subregions is studied in Ramezani et al. (2015).

Aggregating (4) using (1), we obtain:

$$\dot{n}_1(t) = -\frac{n_{11}(t)}{n_1(t)}G_1(n_1(t)) - \frac{n_{12}(t)+n_{10}(t)}{n_1(t)}G_1(n_1(t))u_{12} + \frac{n_{21}(t)}{n_2(t)}G_2(n_2(t))u_{21}(t) + d_1(t), \tag{5a}$$

$$\begin{aligned}\dot{n}_2(t) = &-\frac{n_{22}(t)}{n_2(t)}G_2(n_2(t)) + \frac{n_{12}(t)+n_{10}(t)}{n_1(t)}G_1(n_1(t))u_{12} \\ &-\frac{n_{21}(t)}{n_2(t)}G_2(n_2(t))u_{21}(t) + Q_0(t)u_{02} \\ &-\frac{n_{20}(t)}{n_2(t)}G_2(n_2(t))u_{20}(t) + d_2(t),\end{aligned} \tag{5b}$$

where $d_1(t) = q_{11}(t) + q_{12}(t) + q_{10}(t)$, $d_2(t) = q_{22}(t) + q_{21}(t) + q_{20}(t)$, and $Q_0(t) = Q_{01}(t) + Q_{02}(t)$. In this paper, we assume that the MFD of each region is well-defined and can be approximated with a third-order polynomial:

$$G_i(n_i(t)) = c_{3i}n_i(t)^3 + c_{2i}n_i(t)^2 + c_{1i}n_i(t), \tag{6}$$

where c_{3i}, c_{2i}, and c_{1i} are MFD functional form parameters, $i \in \{1, 2\}$.

2.3. Steady-state condition

The primary step in linearizing the nonlinear dynamics of the system (4) and (5) is to obtain the equilibrium (interchangeably used with steady-state) traffic states n_i^*, n_{ij}^*, and control signals u_k^*, given an estimation of the expected nominal

Please cite this article as: R. Mohajerpoor, M. Saberi and H.L. Vu et al., H_∞ robust perimeter flow control in urban networks with partial information feedback, Transportation Research Part B, https://doi.org/10.1016/j.trb.2019.03.010

values of demand q_{ij}^* and Q_{0i}^* ($i \in \{1, 2\}$, $j \in \Omega_r$, and $k \in \Omega_u$). As such, finding the equilibrium states n_{ij}^* and control signals u_k^* can be carried out by solving the following system of *nonlinear* algebraic equations (8 equations and 12 unknowns):

$$\begin{aligned}
&-\frac{n_{11}^*}{n_1^*}G_1(n_1^*) + \frac{n_{21}^*}{n_2^*}G_2(n_2^*)u_{21}^* + q_{11}^* = 0,\\
&-\frac{n_{22}^*}{n_2^*}G_2(n_2^*) + \frac{n_{12}^*}{n_1^*}G_1(n_1^*)u_{12}^* + Q_{02}^*u_{02}^* + q_{22}^* = 0,\\
&-\frac{n_{12}^*}{n_1^*}G_1(n_1^*)u_{12}^* + q_{12}^* = 0,\\
&-\frac{n_{21}^*}{n_2^*}G_2(n_2^*)u_{21}^* + Q_{01}^*u_{02}^* + q_{21}^* = 0,\\
&-\frac{n_{10}^*}{n_1^*}G_1(n_1^*)u_{12}^* + q_{10}^* = 0,\\
&-\frac{n_{20}^*}{n_2^*}G_2(n_2^*)u_{20}^* + \frac{n_{10}^*}{n_1^*}G_1(n_1^*)u_{12}^* + q_{20}^* = 0,\\
&n_{11}^* + n_{12}^* + n_{10}^* = n_1^*,\\
&n_{22}^* + n_{21}^* + n_{20}^* = n_2^*.
\end{aligned} \tag{7}$$

Note that u_i^* should fulfill constraints (2) and (3), and the last two equations imply that two states are redundant, and can be eliminated resulting in 6 equations and 10 unknowns. In addition, measuring or estimating the nominal (equivalently steady-state) demand q_{ij}^* and Q_{0i}^* is achievable in practice using existing data sources such as vehicles and drivers equipped with GPS devices, and connected vehicles such as taxi fleets Hamedmoghadam-Rafati et al. (2017). The data sources are becoming richer and more accessible every year.

Desired set-point accumulations of each region are ideally defined to maximize the outflow of each region simultaneously, i.e. $n_i^* = n_i^{\mathrm{cr}}$. However, this aim may not be necessarily achievable, because the regions are interconnected, and the SS exogenous demand and constraints on the SS perimeter control signals (defined in (2) and (3)) may force one or both regions to operate in the congested (uncongested) regime, where the SS accumulation is higher (lower) than the critical accumulation. A few papers have studied obtaining optimal set-point accumulations Kouvelas et al. (2017); Kutadinata et al. (2016). Kouvelas et al. Kouvelas et al. (2017) employed an adaptive fine tuning algorithm (a data-driven approach) to update the set-point accumulations in real-time, together with the control parameters. Kutadinata et al. Kutadinata et al. (2016) employed a Nash extremum seeking scheme to update the set-point accumulations in real-time to optimize a certain objective, such as network outflow.

Alternatively, we propose an optimization problem to seek the optimal set-point accumulations n_i^* and n_{ij}^*, and equilibrium perimeter control values u_k^*, $k \in \Omega_u$, given the steady-state (SS) demand q_{ij}^* and Q_{0i}^* while ensuring the SS perimeter control signals are feasible:

$$\begin{aligned}
\underset{n_i^*, n_{ij}^*, u_k^*}{\text{minimize}} \quad & \textstyle\sum_{i=1}^{2} \beta_i (n_i^* - n_i^{\mathrm{d}})^2\\
\text{Subject to : } & (7),\\
& 0 \le \{n_i^*, n_{ij}^*\} \le \alpha_i n_i^{\mathrm{j}},\\
& u_1^{*\min} \le \{u_{12}^*, u_{21}^*\} \le u_1^{*\max},\\
& u_2^{*\min} \le \{u_{02}^*, u_{20}^*\} \le u_2^{*\max},\\
& -\delta_1 \le u_{21}^* - u_{12}^* \le \delta_1,\\
& -\delta_2 \le u_{20}^* - u_{02}^* \le \delta_2,
\end{aligned} \tag{O1}$$

where n_i^{d} is the prescribed desired accumulation of Region i, $u_i^{*\min}$ and $u_i^{*\max}$ are the SS lower and upper bounds of the control signals ($u_i^{\min} \le u_i^{*\min}$ and $u_i^{*\max} \le u_i^{\max}$), $0 < \alpha_i < 1$ is a constant coefficient to specify the maximum allowable SS accumulation of Region $i \in \{1, 2\}$, and β_i is a positive prescribed weighting parameter that characterizes the relative importance of Region i with respect to the other region. If the inner region has the priority to achieve the maximum outflow, then its associated weight, i.e. β_1, should be larger than β_2.

The optimization problem (O1) is nonlinear and non-convex. The non-convexity of the problem arises from the nonlinear equality constraints (7). The problem can be efficiently solved for the local optimal solution via existing nonlinear optimization programs. It is clear that setting the initial set-point accumulations at the desired values, the local optimal solution is conceivably the global optimal one, provided that it is not located far from the desired set-point values. Nevertheless, as long as the solution space is not empty, a local optimal solution can be found.

A special aim could be enforcing the SS accumulation of region i to be exactly equal to its desired value. This could be simply achieved by modifying (O1), through nullifying the associated weighting coefficients ($\beta_i = 0$), and substituting $n_i^* = n_i^{\mathrm{d}}$. Consequently, the program becomes a feasibility problem that might have no solution. This point is further elaborated via an example in Section 4. Nevertheless, if we do not restrict the set-point accumulations to be exactly equal to their

Please cite this article as: R. Mohajerpoor, M. Saberi and H.L. Vu et al., H_∞ robust perimeter flow control in urban networks with partial information feedback, Transportation Research Part B, https://doi.org/10.1016/j.trb.2019.03.010

desired values, the optimization problem (O1) will always find an admissible SS condition that minimizes the objective function in the solution space, unless the feasible solution space defined by the constraints of (O1) is empty. In case the solution space is empty, there will be no feasible control action that can avoid the over-congestion of one or both regions (defined by accumulations $\alpha_i n_i^j$).

2.4. Linearization of dynamic equations

The dynamic model (4) is nonlinear, whereas the proposed controller is a linear controller. Accordingly, the controller design requires the nonlinear model (4) to be first linearized at the equilibrium states, control signals, and demand derived through solving optimization problem (O1). The state space dynamic model of the linearized system is derived in this section.

Let us describe the dynamics of the system using (4a), (4b), (4e), (4f) and (5) as we choose the independent states of the system as n_1, n_2, n_{11}, n_{22}, n_{10}, and n_{20}. The nonlinear dynamics can be written in abstract form as:

$$\dot{n}_i(t) = f_i(n_i, u_k) + d_i(t),$$

where $f_i(n_i,\ u_k)$; $i \in \Omega_n = \{1, 2, 11, 22, 10, 20\}, k \in \Omega_u$, are the nonlinear terms on the right hand side of (4a), (4b), (4e), (4f) and (5), and $d_i(t) = q_i(t),\ i \in \Omega_n \backslash \{1,\ 2\}$. Linearizing the above equations at the SS values of the states, control signals, and demand can be carried out as:

$$\Delta\dot{n}_i(t) = \sum_{j\in\Omega_n} \frac{\partial f_i}{\partial n_j}\Delta n_j(t) + \sum_{k=1}^{s_u} \frac{\partial f_i}{\partial u_k}\Delta u_k(t) + \Delta d_i(t),$$

where $\Delta n_i(t) = n_i(t) - n_i^*,\ i \in \Omega_n,\ \Delta u_k(t) = u_k(t) - u_k^*,\ k \in \Omega_u,\ \Delta d_j(t) = d_j(t) - d_j^*\ (j \in \Omega_n \backslash \{2,\ 22\}),\ \Delta d_2(t) = d_2(t) - d_2^* + (Q_0(t) - Q_0^*)u_{02}^*$, and $\Delta d_{22}(t) = d_{22}(t) - d_{22}^* + (Q_{02}(t) - Q_{02}^*)u_{02}^*$. As such, the linearized dynamics are:

$$\begin{aligned} &\Delta\dot{n}(t) = A\Delta n(t) + B\Delta u(t) + \Delta d(t),\\ &y(t) = C\Delta n(t), \end{aligned} \tag{8}$$

where $\Delta n(t) = [\Delta n_1(t),\ \Delta n_2(t),\ \Delta n_{11}(t),\ \Delta n_{22}(t),\ \Delta n_{10}(t),\ \Delta n_{20}(t)]^T$, $\Delta u(t) = [\Delta u_{12}(t),\ \Delta u_{21}(t),\ \Delta u_{02}(t),\ \Delta u_{20}(t)]^T$, $\Delta d(t) = [\Delta d_1(t), \Delta d_2(t), \Delta d_{11}(t), \Delta d_{22}(t), \Delta d_{10}(t), \Delta d_{20}(t)]^T$, $y(\cdot)$ is the measurement output from the network, $A \in \mathbb{R}^{s_n \times s_n}$, $B \in \mathbb{R}^{s_n \times s_u}$, and $C \in \mathbb{R}^{s_p \times s_n}$ are constant matrices that are obtained from the linearization procedure, $s_n = 6$ is the number of states, $s_u = 4$ is the number of control signals, and s_p is the number of states that are measured in real-time. Detailed expressions of the elements of matrices A and B are given in Appendix A.

In practice, it is challenging to measure the number of vehicles in a region based on their destination region. One of the contributions of this paper is to relax this limitation, in a way that the control framework needs only a subset of the states. In other words, it is possible to measure only one state in real-time, e.g. the accumulation of the inner region, or the full set of states. The number of measured states s_p can vary from 1 to s_n.

Moreover using (2), $\Delta u_i(t)$ is bounded as:

$$-u_i^* < -\Delta u_i^{\min} \le \Delta u_i(t) \le \Delta u_i^{\max} < 1 - u_i^*, \tag{9}$$

where $\Delta u_i^{\max} := u_i^{\max} - u_i^*$ and $\Delta u_i^{\min} := -u_i^{\min} + u_i^* > 0$. It is assumed that the real-time variation of demand $d_i(t)$ from its nominal value is bounded. This constraint can be described as

$$\|\Delta d(t)\|_2 = \sqrt{\int_0^\infty \Delta d^T(s)\Delta d(s)\,\mathrm{d}s} \le \bar{d}, \tag{10}$$

where $\bar{d} \ge 0$ is a constant scalar that represents the maximum expected sum of squared variations of the demand from its nominal value at the steady-state equilibrium.

3. Controller design

The aim of the control strategy is to maintain the accumulation of each region at the desired level by allowing only a fraction of the transfer flows to travel between the regions in real-time. The block diagram of the proposed control architecture is depicted in Fig. 2.

We develop two classes of controllers, (i) P and (ii) PI. The contribution of this section is the design of the control gains for the multi-input multi-state traffic model, guaranteeing the asymptotic stability and robust performance of the network. The controllers are designed for the linearized model (8), and can be applied to the nonlinear system as long as the system does not considerably deviate from the equilibrium state. The numerical experiments in Section 4 show the output of the nonlinear model while the controller is designed based on the linearized model.

The controllers are designed under the assumption of partial information feedback from the network, e.g. only measuring the accumulation of each region, which corresponds to $s_p = 2$ and $C = [I_{s_p}, \mathbf{0}]$. Unmeasured states, i.e. $n_{11}(t)$, $n_{22}(t)$, $n_{10}(t)$, and $n_{20}(t)$, are estimated in real-time using a state observer. To design the observer, it is sufficient that the pair (A, C) be *observable* or *detectable* Brogan (1982). If the system is not observable nor detectable, it is still possible to design a *functional*

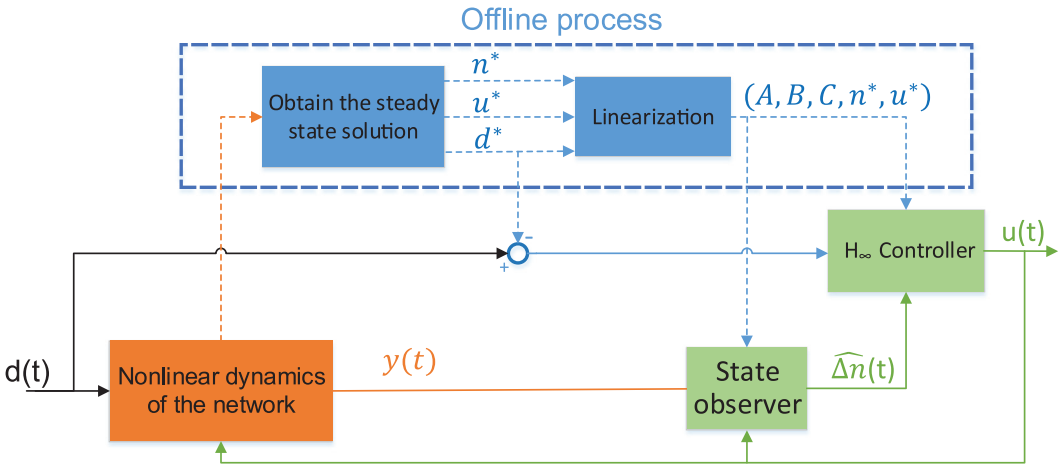

Fig. 2. A block diagram of the P and PI control schemes. The nonlinear dynamics of the network is demonstrated by (1) and (4), and the linearized dynamics are stated in (8). n^*, u^*, and d^* are the vectors of equilibrium states, control inputs, and demand, respectively. The controller aims at the real-time adjustment of the control signals $u_k(t)$, $k \in \Omega_u$, in response to real-time variations of demand using a partial information feedback from the network. Each dashed line indicates that the process is off-line and is not recurrent in real-time, while the solid lines sketch the real-time processes.

observer based controller for the system (see Mohajerpoor et al. (2015b,a) for more information on functional observers), which is a topic for future research.

Remark 1. Note that the origin-destination data is only required in the steady-state condition to define the SS demands q_{ij}^* and Q_{0i}^* ($i \in \{1, 2\}$, $j \in \{1, 2, 3\}$). However, the demand can vary from the SS condition in real-time and the variation is treated as uncertainty/disturbance. The control algorithm only requires the knowledge on the variation bounds of each demand from its SS value to achieve a pre-specified H_∞ robust performance. The data that should be measured in real-time is defined by $y(t)$ in (8), which are the accumulations of each region.

3.1. Proportional (P) controller design

We consider an observer-based P controller as follows:

$$\Delta u(t) = K_P \widehat{\Delta n}(t), \tag{11}$$

where $\widehat{\Delta n}(\cdot) \in \mathbb{R}^{s_n}$ is the estimation of $\Delta n(\cdot)$, and $K_P \in \mathbb{R}^{s_u \times s_n}$ is the proportional gain to be designed. A full-state Luenberger observer is considered to estimate the states of the linearized system (8) Brogan (1982):

$$\dot{\widehat{\Delta n}}(t) = A\widehat{\Delta n}(t) + L(y(t) - C\widehat{\Delta n}(t)) + B\Delta u(t), \tag{12}$$

where $L \in \mathbb{R}^{s_n \times s_p}$ is the observer parameter to be designed. Therefore, the observation error $e_y(t) \triangleq \widehat{\Delta n}(t) - \Delta n(t)$ has the following dynamics:

$$\dot{e}_y(t) = (A - LC)e_y(t) - \Delta d(t). \tag{13}$$

Let us define $x_P(t) := [\Delta n(t)^T, e_y^T(t)]^T \in \mathbb{R}^{2s_n}$. Accordingly, dynamic Eqs. (8), (11) and (13) can be augmented as

$$\begin{aligned} \dot{x}_P(t) &= A_P x_P(t) + D_P \Delta d(t), \\ z(t) &= C_P x_P(t), \end{aligned} \tag{14}$$

where $z(\cdot)$ is the controlled output,

$$A_P = \begin{bmatrix} A + BK_P & BK_P \\ \mathbf{0} & A - LC \end{bmatrix}, \; D_P = \begin{bmatrix} I_{s_n} \\ -I_{s_n} \end{bmatrix}, \text{ and } C_P = [I_{s_n}, \mathbf{0}].$$

Definition 1. The system (14) is *globally uniformly asymptotically stable* (GUAS), if the equilibrium point $x_P(t) \equiv 0$ of the system with $\Delta d \equiv 0$ is GUAS.

In addition to the asymptotic stability, the controller aims to achieve the H_∞ performance criteria defined below.

Definition 2. System (14) is H_∞ robustly stable, if under zero initial conditions we have $J_\gamma \leq 0$, where $J_\gamma = \int_0^\infty \left(z^T(s)z(s) - \gamma^2 \Delta d^T(s)\Delta d(s)\right)ds$ for some $\gamma > 0$ Apkarian and Noll (2006).

The robustness gain γ characterises the capability of the controller in damping out the effect of disturbance terms. The lower the admissible gain γ, the better performance can be achieved from applying the robust controller. The following theorem summarizes the proposed design procedure for controller (11)-(12).

Please cite this article as: R. Mohajerpoor, M. Saberi and H.L. Vu et al., H_∞ robust perimeter flow control in urban networks with partial information feedback, Transportation Research Part B, https://doi.org/10.1016/j.trb.2019.03.010

Theorem 1. *Consider the linearized dynamics (14). Let L be designed in a way that the eigenvalues of matrix $A_c = A - LC$ are placed arbitrarily in the negative half of the s-plane. Given $\bar{d} > 0$ and δ_i, $i = \{1, 2\}$, if there exist positive definite matrices W_1 and $P_2 \in \mathbb{S}^{s_n \times s_n}$, and any matrices K_P and $Z_P \in \mathbb{R}^{s_u \times s_n}$, such that the following LMIs and equality constraint are satisfied, then the system is globally uniformly asymptotically stable.*

$$\begin{bmatrix} \mathrm{He}(AW_1 + BZ_P) & BK_P \\ * & \mathrm{He}(P_2 A_c) \end{bmatrix} \prec 0, \tag{15}$$

$$\begin{bmatrix} \frac{1}{2\rho}\tilde{u}_\nu W_1 & \mathbf{0} & Z_P^T \mathbf{e}_\nu^T \\ * & \frac{1}{2\rho}\tilde{u}_\nu P_2 & K_P^T \mathbf{e}_\nu^T \\ * & * & 1 \end{bmatrix} \succeq 0 \qquad \nu = \{1, \cdots, \boldsymbol{s_u}\}, \tag{16}$$

$$\begin{bmatrix} \frac{4\delta_i^2}{\rho} W_1 & \mathbf{0} & Z_P^T C_{u_i}^T \\ * & \frac{4\delta_i^2}{\rho} P_2 & K_P^T C_{u_i}^T \\ * & * & 1 \end{bmatrix} \succeq 0 \qquad i = \{1, 2\}, \tag{17}$$

$$Z_P - K_P W_1 = \mathbf{0}, \tag{18}$$

where $\tilde{u}_\nu \triangleq \Delta u_\nu^{\max 2} - \Delta u_\nu^{\min 2} + 2\Delta u_\nu^{\min} \Delta u_\nu^{\max}$, $\rho = \gamma^2 \bar{d}^2 + V(0)$, $C_{u_1} = [-1, 1, 0, 0]$, $C_{u_2} = [0, 0, -1, 1]$, and $V(t)$ is the Lyapunov function defined in (B.1). The system is further H_∞ robustly stable, if the additional LMI below is satisfied for given $\gamma > 0$:

$$\begin{bmatrix} \mathrm{He}(AW_1 + BZ_P) & W_1 & BK_P & I_{s_n} \\ * & -I_{s_n} & \mathbf{0} & \mathbf{0} \\ * & * & \mathrm{He}(P_2 A_c) & -P_2 \\ * & * & * & -\gamma^2 I_{s_n} \end{bmatrix} \prec 0. \tag{19}$$

Proof. The theorem is proved in Appendix B. □

The LMI (15)-(19) are not convex due to the nonlinear constraint (18). To resolve this problem, we propose a modified Cone Complementary Algorithm (CCA) Ghaoui et al. (1997), as Algorithm 1. Steps (ii) and (v) of the algorithm are added

Algorithm 1 Modified CCA for designing the control matrix K_P.

(i) Initialization: Solve LMIs (15), (16), (17), and (19) for W_1, K_P for given $\gamma > 0$, and Z_P, and set $W_1^0 = W_1$ and $K_P^0 = K_P$.

(ii) Define $\tilde{K}_P = Z_P^0 W_1^{0^{-1}}$. If LMIs (15), (16), (17) and (19) are feasible with $K_P = \tilde{K}_P$, W_1, and Z_P, then choose $K_P = \tilde{K}_P$ and exit the algorithm. Otherwise, proceed to Step (iii).

(iii) Iteration $k > 0$: If $k > k_{\max}$, with $k_{\max} > 0$ as a sufficiently large threshold criterion, then the algorithm does not return any solution and terminates. Otherwise, solve the following convex optimization problem for W_1, K_P, and Z_P

$$\begin{aligned} &\underset{W_1, K_P, Z_P}{\text{minimize}} \quad \|K_P^k W_1 + K_P W_1^k - 2Z_P\|_F \\ &\text{Subject to: (15), (16), (17), and (19).} \end{aligned} \tag{O2}$$

(iv) If replacing K_P by $\tilde{K}_P = Z_P {W_1}^{-1}$ still satisfies LMIs (15), (16), (17), and (19), then $K_P \leftarrow \tilde{K}_P$, and exit the algorithm. Otherwise, proceed to Step (v).

(v) If $\|K_P^k W_1 + K_P W_1^k - 2Z_P\|_F < \tilde{\delta}$, with $\tilde{\delta} > 0$ as a sufficiently small threshold criterion, then $K_P \leftarrow K_P^k$ and stop. Otherwise, $k \leftarrow k + 1$, $K_P^k \leftarrow K_P$ and $W_1^k \leftarrow W_1$, and return to Step (iii).

with respect to the original CCA to accelerate the convergence rate of the algorithm. If the algorithm does not converge, e.g. by breaching the maximum iteration criterion, then one can sacrifice the controller's performance by increasing γ, and repeat the algorithm until a feasible solution is obtained.

Remark 2. There are two sources of inaccuracies with an MFD-based dynamic model of a network: 1. uncertainties in demand estimation (modelled as $\Delta d(t)$ in the paper) and 2. uncertainties and inaccuracies of the MFD model, which are partly due to the heterogeneity of the network density. The paper focuses on the first source of uncertainties, while treating the second source of inaccuracy (i.e. model uncertainties) can follow the same methodology proposed here. However, the modelling and controller design procedure should be amended to cope with this extra complexity. Moreover, through modelling the MFD heterogeneity (as in Ramezani et al. (2015)), one can predict the behaviour of the network, instead of treating the deviations from the ideal MFD shape as uncertainties. Studying this topic is a crucial future work.

Please cite this article as: R. Mohajerpoor, M. Saberi and H.L. Vu et al., H_∞ robust perimeter flow control in urban networks with partial information feedback, Transportation Research Part B, https://doi.org/10.1016/j.trb.2019.03.010

3.2. Proportional-Integral (PI) controller design

We consider an observer-based PI controller as follows:

$$\Delta u(t) = K_P \widehat{\Delta n}(t) + K_I \int_0^t \widehat{\Delta n}(s)\mathrm{d}s, \tag{20}$$

where $K_P, K_I \in \mathbb{R}^{s_u \times s_n}$ are the proportional and integral gains to be designed, respectively. Note that K_P in the P controller (11) and PI controller (20) should be distinguished.

Let us define $x_{PI}(t) := [\Delta n(t)^T, e_y^T(t), \Delta u(t)^T]^T \in \mathbb{R}^{(2s_n+s_u)\times 1}$. Accordingly, dynamic Eqs. (8), (13) and (20) can be augmented with

$$\begin{aligned} \dot{x}_{PI}(t) &= A_{PI}x_{PI}(t) + D_{PI}\Delta d(t), \\ z(t) &= C_{PI}x_{PI}(t), \end{aligned} \tag{21}$$

where

$$A_{PI} = \begin{bmatrix} A & \mathbf{0} & B \\ \mathbf{0} & A_c & \mathbf{0} \\ K_PA + K_I & K_PA_c + K_I & K_PB \end{bmatrix}, \; D_{PI} = \begin{bmatrix} I_{s_n} \\ -I_{s_n} \\ \mathbf{0} \end{bmatrix},$$

and $C_{PI} = [I_{s_n}, \mathbf{0}]$. Similar definitions of GUAS and H_∞ robust stability as given in Definitions 1 and 2 are applied to (21). The following theorem describes our method to design the observer-based PI controller.

Theorem 2. *Consider the linearized dynamics (21). Let L be designed in a way that the eigenvalues of matrix $A_c = A - LC$ are placed arbitrarily in the negative half of the s-plane. Given $\bar{d} > 0$ and δ_i, $i = \{1, 2\}$, if there exist positive definite matrices $P_i \in \mathbb{S}^{s_n \times s_n}$, $P_3 \in \mathbb{S}^{s_u \times s_u}$, and any matrices $Z_j \in \mathbb{R}^{s_u \times s_n}$, $j = \{P, I\}$, such that the following LMIs are satisfied, then the system is globally uniformly asymptotically stable.*

$$\begin{bmatrix} \mathrm{He}(P_1A) & \mathbf{0} & P_1B + A^TZ_P^T + Z_I^T \\ * & \mathrm{He}(P_2A_c) & A_c^TZ_P^T + Z_I^T \\ * & * & \mathrm{He}(Z_PB) \end{bmatrix} \prec 0, \tag{22}$$

$$\begin{bmatrix} \frac{1}{2\rho}\tilde{u}_\nu P & \tilde{C}_\nu^T \\ * & 1 \end{bmatrix} \succeq 0 \qquad \nu = \{1, \cdots, s_u\}, \tag{23}$$

$$\begin{bmatrix} \frac{4\delta_i^2}{\rho}\tilde{u}P & \tilde{C}_{PI}^TC_{u_i}^T \\ * & 1 \end{bmatrix} \succeq 0 \qquad i = \{1, 2\}, \tag{24}$$

where $P = \mathrm{diag}(P_1, P_2, P_3)$, $\tilde{C}_{PI} = [\mathbf{0}, I_{s_u}]$, $\tilde{C}_\nu = [\mathbf{0}, \mathbf{e}_\nu]$, $\tilde{u} = [\tilde{u}_1, \cdots, \tilde{u}_{s_u}]^T$, and $\tilde{u}_\nu$, ρ, and C_{u_i} are as defined in Theorem 1. The system is further H_∞ robustly stable, if the additional LMI below is satisfied for given $\gamma > 0$:

$$\begin{bmatrix} \mathrm{He}(P_1A) + I_5 & \mathbf{0} & P_1B + A^TZ_P^T + Z_I^T & P_1 \\ * & \mathrm{He}(P_2A_c) & A_c^TZ_P^T + Z_I^T & -P_2 \\ * & * & \mathrm{He}(Z_PB) & \mathbf{0} \\ * & * & * & -\gamma^2 I_{s_n} \end{bmatrix} \prec 0. \tag{25}$$

Ultimately, the control gains can be obtained from $K_P = P_3^{-1}Z_P$ and $K_I = P_3^{-1}Z_I$.

Proof. The proof is given in Appendix C. □

Remark 3. Note that the observer gain L could also be obtained from the LMI problems in Theorems 1 and 2 (see Wang et al. (1992); Boukal et al. (2017) for more information). However, the performance of the observer influences the performance of the controlled system, as the controller acts more accurately when it is fed by the actual values of the states of the system. Hence, to enable the full adjustment of the observer's performance, L has been obtained via a pole-placement technique Brogan (1982).

Remark 4. The robust performance index γ is assumed to be predefined in Theorems 1 and 2. However, as γ appears linearly in the LMIs, its least admissible value can be obtained from a minimization program, e.g. the feasibility problem (22)-(25) converts to minimization of γ subject to (22)-(25)

Remark 5. It is clear that the criteria of Theorems 1 and 2 do not guarantee the existence of a solution, as there might be no admissible stabilizing controller for the network given the initial accumulations, steady-state solution, bounds on the control signals, and the magnitude of demand disturbances (see Zhong et al. (2018a) for more information). Moreover, to derive the LMIs corresponding to boundedness of the control signals and their differences, a few conservative assumptions are made. First, $\dot{V}(t) + z^T(t)z(t) - \gamma^2\Delta d^T(t)\Delta d(t) < 0$ is approximated by $\dot{V}(t) - \gamma^2\Delta d^T(t)\Delta d(t) < 0$ in obtaining (B.5) and (B.10). Second, Young's inequality is used in obtaining (B.6) and (B.9). These make the criteria of each theorem a sufficient stability condition (as opposed to the necessary and sufficient condition). Further relaxing conditions (16) and (17) in Theorem 1 and conditions (23) and (24) in Theorem 2 is a future direction of this research.

Please cite this article as: R. Mohajerpoor, M. Saberi and H.L. Vu et al., H_∞ robust perimeter flow control in urban networks with partial information feedback, Transportation Research Part B, https://doi.org/10.1016/j.trb.2019.03.010

Table 1
Parameters of the MFD of the regions.

Region	n^{cr}[veh]	n^{j}[veh]	c_3	c_2	c_1
1	3200	8450	3.5×10^{-11}	-7.1×10^{-7}	0.0035
2	4000	12,000	2.46×10^{-11}	-5.9×10^{-7}	0.0036

Remark 6. A problem with regular PID controllers is their reaction delay in accommodating abrupt, unpredicted, and significant demand disturbances. As such, designing proactive controllers, such as predictive PID controllers (Katebi and Moradi (2001)) is an important future line of research. Furthermore, setting the desired accumulation of each region slightly lower than the critical accumulation (e.g. $n_i^{d} = 0.9n_i^{cr}$, $i = \{1, 2\}$), can protect the region from becoming over-congested. This strategy is useful, because each region has the capacity to accommodate the unavoidable increase in the region's accumulation from its set-point due to the abrupt and unforeseen increase of the demand.

Remark 7. The developed control algorithm can be readily extended to a network with multiple concentric regions, or multi-region networks with different topologies. In light of that, the number of states and control inputs of the system increases, and the nonlinear dynamics of the system (4) should be modified. However, obtaining the steady-state condition, as well as the linearization can follow the same procedure proposed here. Accordingly, the linearized dynamics can still be represented in the form of (8), and the proposed controller design algorithms proposed in Theorems 1 and 2 remain valid. Another challenge is clustering the network into multiple homogeneous regions (see e.g. Ji and Geroliminis (2012); Saeedmanesh and Geroliminis (2017)). Studying a large complex network comprising multiple regions is a future research direction.

3.3. Pseudo bang-Bang control algorithm

As a benchmarking control algorithm, this section proposes a bang-bang type control scheme that switches each control signal u_k ($k \in \Omega_u$) between their maximum and minimum values, while keeping the bounded difference of the control signals on each perimeter (i.e. Conditions (3)). We name the algorithm a *pseudo bang-bang* (PBB) control method, since unlike other bang-bang algorithms the control signals could take values less than their maximum, or greater than their minimum admissible magnitudes. The aim of this nonlinear controller is regulating the accumulation of each region at the SS value. The PBB algorithm is illustrated in Appendix D.

4. Numerical experiments and discussions

This section presents the results of numerical experiments on the hypothetical road network depicted in Fig. 1. The critical and jam accumulations, as well as the MFD parameters of each region are listed in Table 1 and the MFDs are plotted in Fig. 3. Note that the desired accumulation of each region should be chosen to be close and slightly lower than the

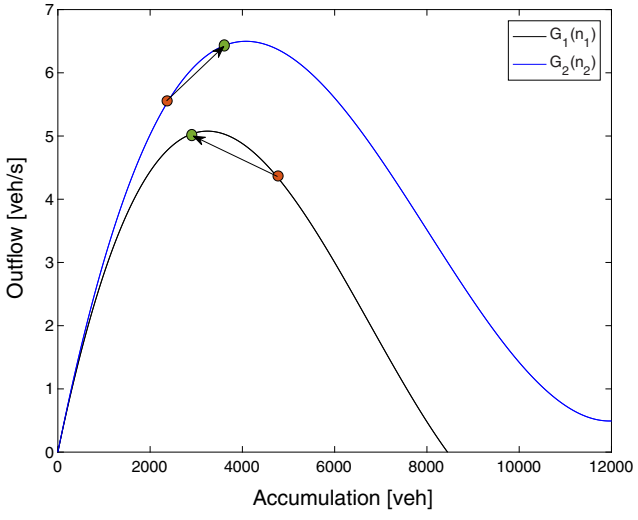

Fig. 3. MFDs of the studied regions. Initial accumulation of each region is highlighted with a red circle, and the desired accumulation of each subnetwork ($0.9n_i^{cr}$) is highlighted with a green circle. (For interpretation of the references to colour in this figure legend, the reader is referred to the web version of this article.)

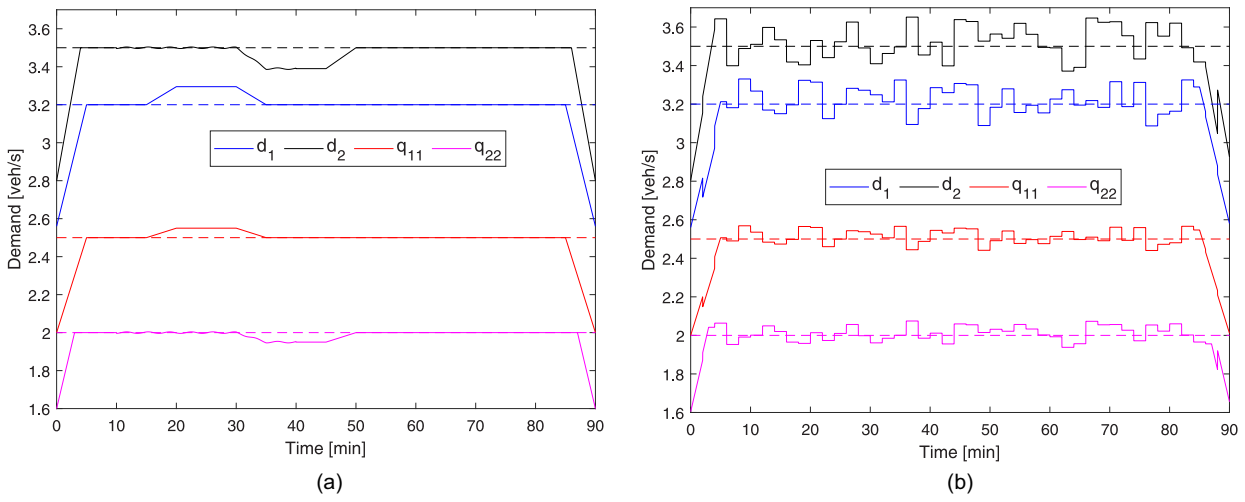

Fig. 4. Real-time demand during the simulation period. Each demand profile rises to its nominal value first (loading regime), then fluctuates around the nominal value, and finally drops (unloading regime). (a) Demand with moderate disturbances to show the asymptotic stability and robustness properties of the controllers. (b) Demand with heavy disturbances to examine the effectiveness and robustness of the control algorithms under more severe and persistent demand fluctuations. Each SS demand is highlighted via a dashed line. Note that $d_1(t) = q_{11}(t) + q_{12}(t) + q_{10}(t)$, $d_2(t) = q_{22}(t) + q_{21}(t) + q_{20}(t)$, and $q_{10}(t)$ and $q_{20}(t)$ are not shown for the sake of presentation quality of the other demand components in the figure.

corresponding critical accumulation. This is first to maximize the region outflow as much as possible and second to accommodate the fluctuations in the region's accumulation, which can stem from the delay of the controllers in reacting to demand disturbances. Hence, the desired accumulations of each region is considered as 90% of its critical accumulation, i.e. $n_i^{\mathrm{d}} = 0.9 n_i^{\mathrm{cr}}$, $i = \{1, 2\}$. The initial accumulations of the regions are arbitrarily selected as $n_1(0) = 1.5 n_1^*$ and $n_2(0) = 0.8 n_2^*$, i.e. Region 1 and Region 2 are initially congested and uncongested, respectively. The initial accumulations are chosen far from the equilibrium states to better examine the effects of the nonlinearity of the dynamics.

Let us assume that during the studied peak period, which lasts 90 minutes, the SS demands are estimated or measured as $q_{11}^* = 2.5$ [veh/s], $q_{22}^* = 2$ [veh/s], $q_{12}^* = 0.6$ [veh/s], $q_{21}^* = 1.2$ [veh/s], $q_{10}^* = 0.1$ [veh/s], $q_{20}^* = 0.3$ [veh/s], $Q_{01}^* = 0.8$ [veh/s], and $Q_{02}^* = 0.6$ [veh/s]. This indicates that the inner region has a higher internal and transfer flow demand in the steady-state.

Three case studies are considered: (i) loading each region with moderately-fluctuating demand demonstrated in Fig. 4(a) and setting $\delta_i = 0.3$; (ii) loading each region as in Case study (i) and setting $\delta_i = 0$, $i = \{1, 2\}$; and (iii) loading each region with heavily-fluctuating demand demonstrated in Fig. 4(b) and setting $\delta_i = 0.3$. Case study (i) aims to demonstrate the effectiveness of the proposed controllers in robustly asymptotically stabilizing the network. Case study (ii) investigates the potential impacts of reducing the degrees of freedom of the controller by setting $\delta_i = 0$. Note that $\delta_i = 0$ necessitates that $u_{12}(t) = u_{21}(t)$ and $u_{02}(t) = u_{20}(t)$ at all times. The PBB algorithm in all case studies uses the actual values of the internal states, whereas the P and PI controllers employ the estimated states (obtained from observer (12)) in their structures. Furthermore, case study (iii) elucidates the performance and robustness of the control algorithms when facing severe consistent random variations in the demand.

Throughout the section it is assumed that the SS control signals are at least 0.4 and at most 0.7, i.e. $u_i^{*\min} = 0.4$ and $u_i^{*\max} = 0.7$, and in solving (O1) $\beta_i = 1$ and $\alpha_i = 0.9$ ($i = \{1, 2\}$). Note that larger control signals u_k, $k \in \Omega_u$, lead to higher transfer flows and potentially larger trip completion rates. Hence, it is highly desirable that the SS control signals be as close as possible to 1, provided that there exists a solution to the optimization problem (O1) such that the SS accumulations are sufficiently close to the desired accumulations. Moreover, the real-time lower and upper bounds of the control signals are fixed at $u_i^{\min} = 0.2$ and $u_i^{\max} = 0.9$. Further, it is assumed that only the accumulation of each region is measured in real-time, i.e. $C = [I_2, \mathbf{0}]$.

We investigate the performance of the proposed perimeter control algorithms on the *nonlinear*, dynamics (4) considering five different perimeter control strategies: (i) robust P controller with best achievable performance, (ii) robust PI controller with best achievable performance, (iii) the PBB control algorithm (Algorithm 2) (iv) the SS control signals $u_k(t) = u_k^*$ ($k = \Omega_u$), and (v) no real-time control by fixing $u_k = 0.9$ (called fixed control hereafter), allowing no dynamic control of the transfer flows between regions.

4.1. Case study (i)

As a first step, solving the optimization problem (O1) results in the SS accumulations and control signals, $n_i^* = n_i^{\mathrm{d}}$ ($i = \{1, 2\}$), $n_{11}^* = 2504$ [veh], $n_{22}^* = 2078$ [veh], $n_{12}^* = 346$ [veh], $n_{21}^* = 1231$ [veh], $n_{10}^* = 30$ [veh], $n_{20}^* = 291$ [veh], $u_{12}^* = 0.61$, $u_{21}^* = 0.53$, $u_{02}^* = 0.69$, and $u_{20}^* = 0.64$. The algorithm is quite efficient in finding the SS solution, and it only took 7 iterations to find the optimal solution.

Please cite this article as: R. Mohajerpoor, M. Saberi and H.L. Vu et al., H_∞ robust perimeter flow control in urban networks with partial information feedback, Transportation Research Part B, https://doi.org/10.1016/j.trb.2019.03.010

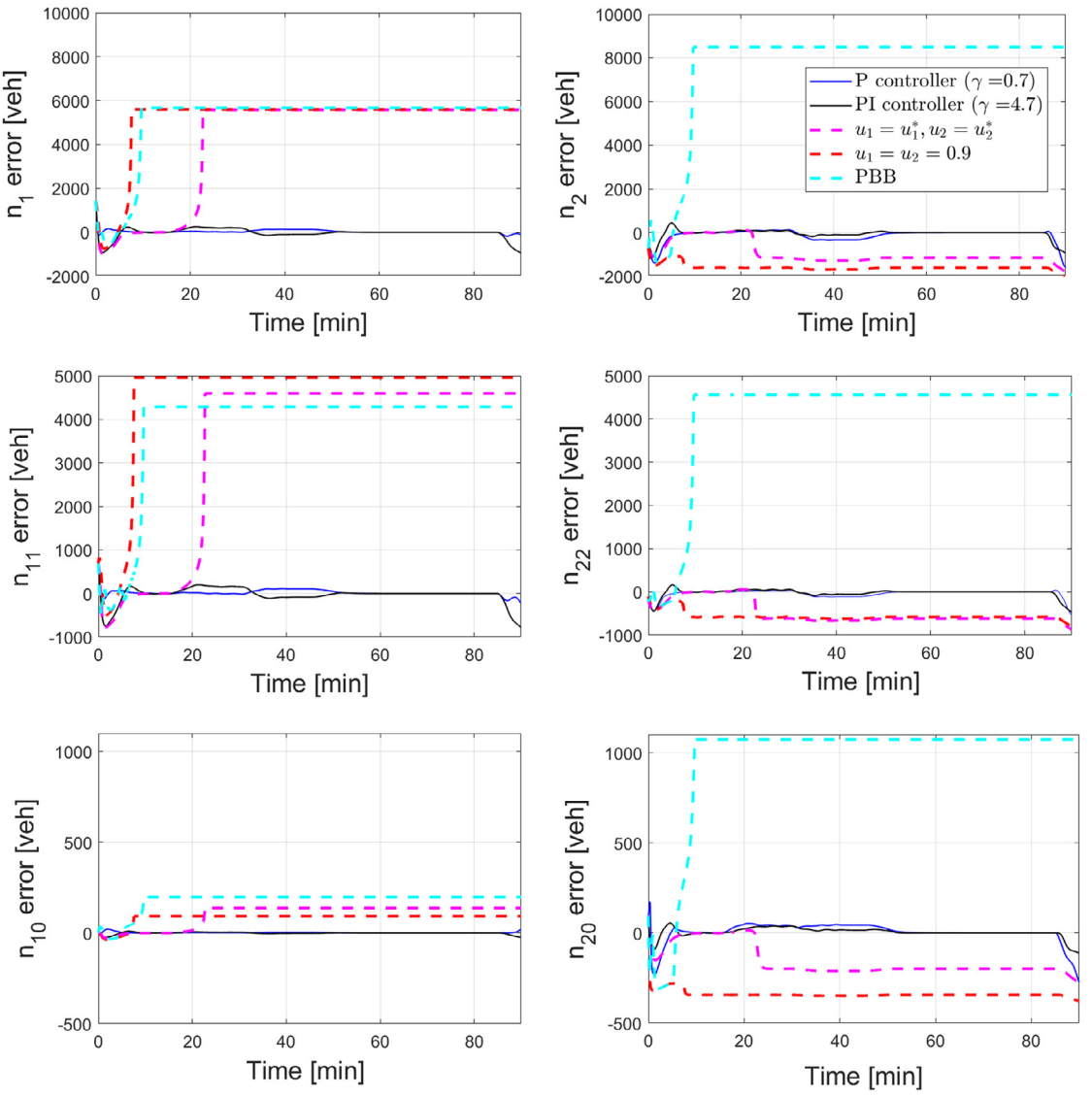

Fig. 5. Variations of accumulation errors $(n_i(t) - n_i^*,\ i \in \Omega_n)$ of Regions 1 and 2 under various controllers applied to the nonlinear model in case study (i): 1. robust P controller with best achievable robust performance ($\gamma = 0.7$), 2. robust PI controller with best attainable robust performance ($\gamma = 4.7$), 3. PBB control algorithm (Algorithm 2), 4. the SS control signals $(u_k(t) = u_k^*,\ k \in \Omega_u)$, and 5. fixed control $u_k = 0.9$. The PBB algorithm employs the actual states in examining Conditions I and II used in Algorithm 2.

Characteristic matrices A and B obtained from linearizing the nonlinear dynamics (1), (4), (5), and (6) at the nominal equilibrium states, control signals, and demand are reported in Appendix E. We placed the closed-loop poles of the observer dynamics arbitrarily at $[-8.8 - 8.6 - 8.2 - 8.3 - 8.4 - 8.7]$. Thereafter, applying the criterion of Theorem 1 and Algorithm 1 to design the proportional controller, we obtain the best admissible performance of $\gamma = 0.7$. Moreover, applying the criterion of Theorem 2 to design the PI controller, the best admissible performance of $\gamma = 4.7$ is achieved. The attained observer and control parameters are presented in Appendix E.

Simulation results from implementing control strategies (i-v) conducted in a MATLAB environment are demonstrated in Figs. 5 to 10. Fig. 5 shows the accumulation errors (i.e. Δn_i and Δn_{ij}) of the controlled regions with different control strategies. Moreover, Fig. 6 highlights the MFDs when adopting various control strategies. According to the figures, with the SS and fixed control strategies (strategies (iv) and (v)), Region 1 (which is the destination of most of the trips) becomes heavily congested and faces gridlock. This emphasizes the importance of dynamic control actions. Moreover, the heuristic PBB controller has resulted in the gridlock of both regions. On the other side, through applying the robust P and PI dynamic controllers, the accumulations essentially remain close to their desired values when the disturbances are nonzero, and their errors asymptotically converge to zero when $\Delta d(t) = 0$. This leads to the maximum outflow of the whole network as emphasized in Figs. 6 and 10.

Please cite this article as: R. Mohajerpoor, M. Saberi and H.L. Vu et al., H_∞ robust perimeter flow control in urban networks with partial information feedback, Transportation Research Part B, https://doi.org/10.1016/j.trb.2019.03.010

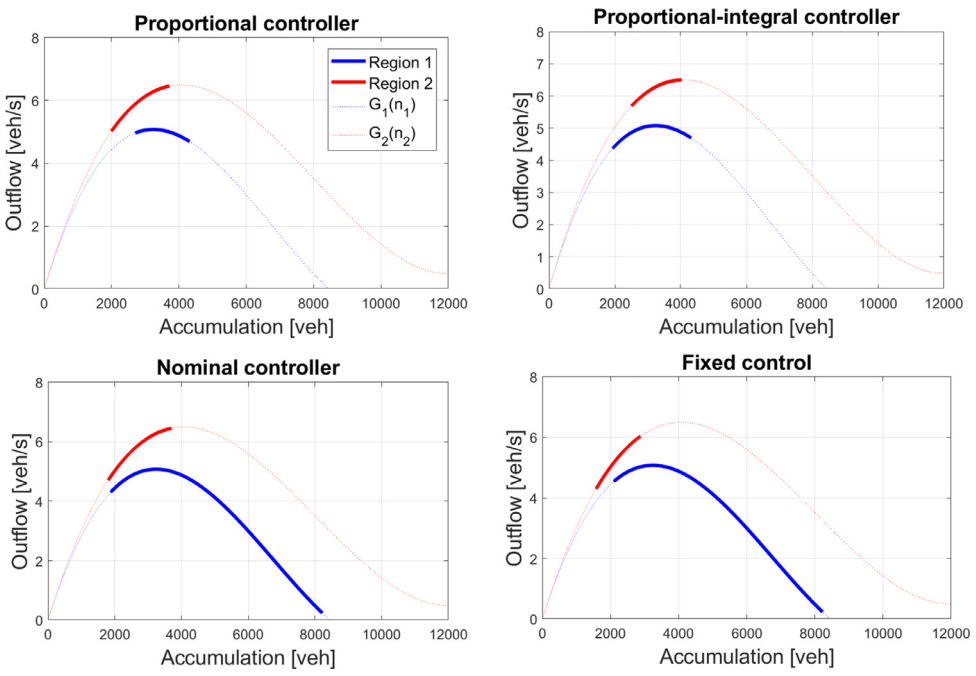

Fig. 6. The MFD of each region for different control strategies in case study (i): 1. robust P controller with best attainable performance at $\gamma = 0.7$, 2. robust PI controller with best achievable performance at $\gamma = 4.7$, 3. constant nominal SS control signals $u_k(t) = u_k^*$ ($k \in \Omega_u$), and 4. fixed control $u_k = 0.9$. It is observed that the designed real-time controllers enable maintaining the accumulation of each subnetwork around their desired accumulations, while the SS control signals and fixed control strategies lead to the gridlock of Region 1.

Fig. 7 shows the dynamic perimeter control signals at each perimeter with robust P and PI control strategies and the PBB framework. Moreover, Fig. 8 shows the difference between the P and PI control signals on each perimeter during the experiment, which highlights that the differences remain within the defined threshold of $\delta_i = 0.3$. The comparison of the robust P and PI controllers in Figs. 5, 7, and 8 suggests that the criterion to design the robust P controller obtains superior robust performance due to achieving a lower minimum admissible γ. As such, the robust PI controller is slower in addressing the disturbance effects, but has satisfied constraints (2) and (3) (see Figs. 7 and 8). The shortcoming of the PI controller can be addressed in future research studies via proposing a less conservative stability criterion (see Remark 3). It is worth highlighting that the PBB controller results in a undesirable high switching rate around $t = 10$ [min] for the first perimeter.

Fig. 9 plots the state estimation errors, where the state estimations for the linearized model (8) obtained from (12) are compared against their actual values from the nonlinear model (4). It can be seen that the errors are bounded when $\|\Delta d(t)\| > 0$ and quickly converge to zero when $\Delta d(t) = 0$. Accordingly, the observer effectively estimates the unknown accumulations in real-time.

Fig. 10 shows the cumulative trip completion of control strategies (i)-(v). Note that the total trip completion rate of the network is the sum of the trip completion rate of each region (internal outflow) plus the outflow from Region 2 to the outer region 0 (external outflow). Accordingly, the cumulative total trip completion of the network can be expressed as the integration of the total trip completion rate as follows:

$$\int_0^t \left(\sum_{i=1}^{2} \frac{n_{ii}(s)}{n_i(s)} G_i(n_i(s)) + \frac{n_{20}(s)}{n_2(s)} G_2(n_2(s)) \right) \mathrm{d}s.$$

Comparing the control strategies in Fig. 10 indicates that the PBB control strategy imposes the highest delays on the network's vehicles. Note that the area between the curves associated with the trip completions of two control strategies corresponds to the total extra delay implied due to applying a strategy compared to the other (the strategy with lower trip completion imposes further delays). On the other hand, the robust P and PI controllers have shown similar performances and they outperform other strategies in minimizing the total delay of the network. The proportional controller has performed slightly better than the PI controller as shown in the right sub-figure of the figure.

Note that the PBB controller is heuristic and unlike the P and PI controllers its robustness is not guaranteed. The performance of the PBB controller depends sensitively on the steady-state and demand perturbation, and it might even outperform the robust P and PI controllers in certain conditions like scenarios wherein the rate of the transfer flow to the internal flow demand is low. The robust performance of the PBB controller can be adjusted and improved by designing its switching rule based on a stability or optimization objective criterion (see e.g. Aalipour et al. (2018)).

Please cite this article as: R. Mohajerpoor, M. Saberi and H.L. Vu et al., H_∞ robust perimeter flow control in urban networks with partial information feedback, Transportation Research Part B, https://doi.org/10.1016/j.trb.2019.03.010

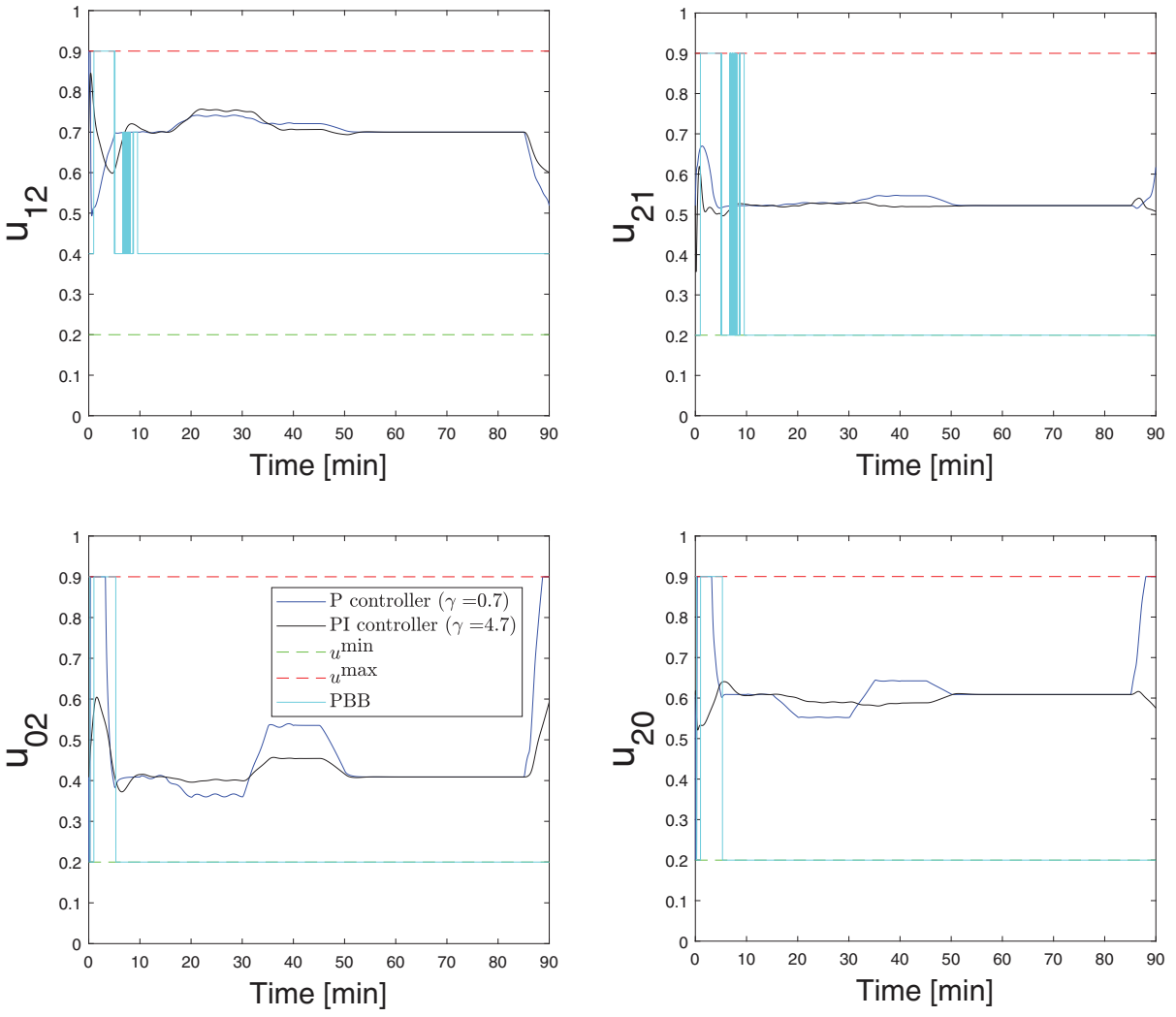

Fig. 7. Perimeter control signals with robust P, PI, and PBB control strategies applied to the nonlinear model for Case study (i). The minimum and maximum admissible control values are shown by black and red dashed lines, respectively. (For interpretation of the references to colour in this figure legend, the reader is referred to the web version of this article.)

4.2. Case study (ii)

In this case study, we assume $\delta_i = 0$, which reduces the controller's DoF from 4 to 2, i.e. perimeter control signals operating on a perimeter have identical values for both directions. Accordingly, and due to fixing the minimum allowable SS control signals at $u_i^{*\min} = 0.4$, the optimization problem (O1) could not return the desired accumulations as the SS accumulations. The SS accumulations and control signals are obtained as $n_1^* = n_1^{\mathrm{d}} + 211$ [veh], $n_2^* = n_2^{\mathrm{d}} - 617$ [veh], $n_{11}^* = 2451$ [veh], $n_{22}^* = 1385$ [veh], $n_{12}^* = 548$ [veh], $n_{21}^* = 1110$ [veh], $n_{10}^* = 91$ [veh], $n_{20}^* = 488$ [veh], $u_{12}^* = u_{21}^* = 0.67$, and $u_{02}^* = u_{20}^* = 0.40$.

Applying Theorems 1 and 2 result in control gains for the observer-based robust P and PI controllers with lowest admissible performance gains of $\gamma = 0.7$ and $\gamma = 15.5$, respectively. The results shown in Figs. 11, 12, 13 indicate that only the P controller has been successful in regulating the accumulations of each region at the SS values. In summary, the PI, SS, and fixed control scenarios result in the gridlock of Region 1, and the PBB controller result in the gridlock of both regions. This case study shows that there exists the opportunity to fully equalize the green times of opposite gated movements without losing the performance of the control strategy. Nevertheless, we observe possible aftereffects of losing the controller's DoF rising from this assumption on the performance of the PI controller. Fig. 10 shows that the Proportional controller has resulted in the lowest network delay, and the PI controller has had a slightly better performance than the SS control scenario as the second best control scenario. Note that the proposed robust P and PI controllers guarantee a *global* stability performance when they are applied to the linearized model. Nevertheless, their effectiveness holds *locally* for the actual nonlinear model (4). Four factors could have critical impacts on the performance of the controllers when applied to the actual non-

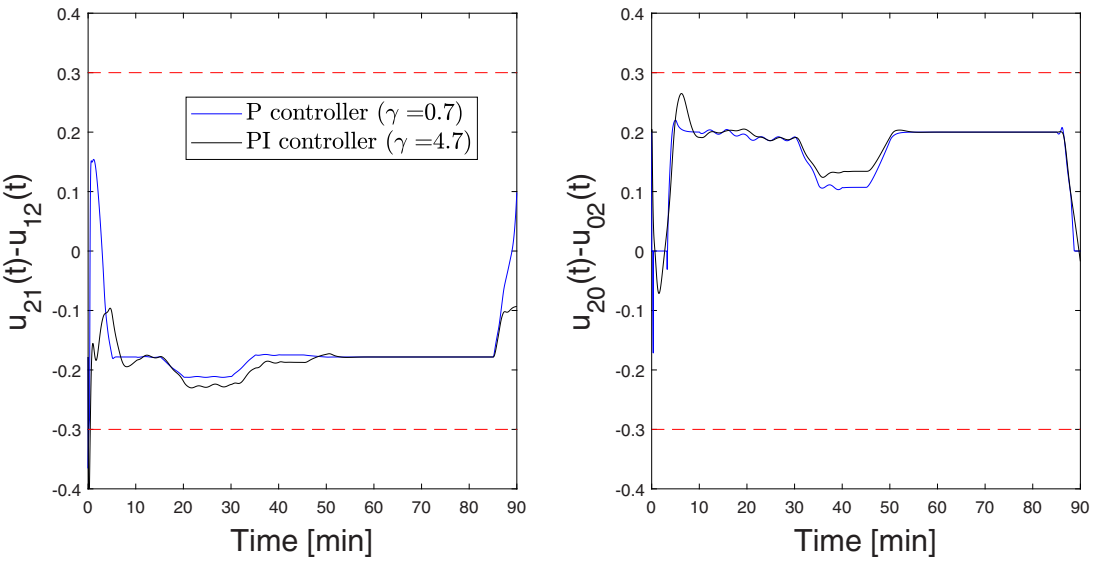

Fig. 8. The difference of the inbound and outbound control signals on perimeters 1 (left figure) and 2 (right figure) during the simulations of case study (i), when applying the robust P and PI controllers. The desired admissible bounds of the difference are highlighted by red dashed lines ($\delta_i = 0.3$). (For interpretation of the references to colour in this figure legend, the reader is referred to the web version of this article.)

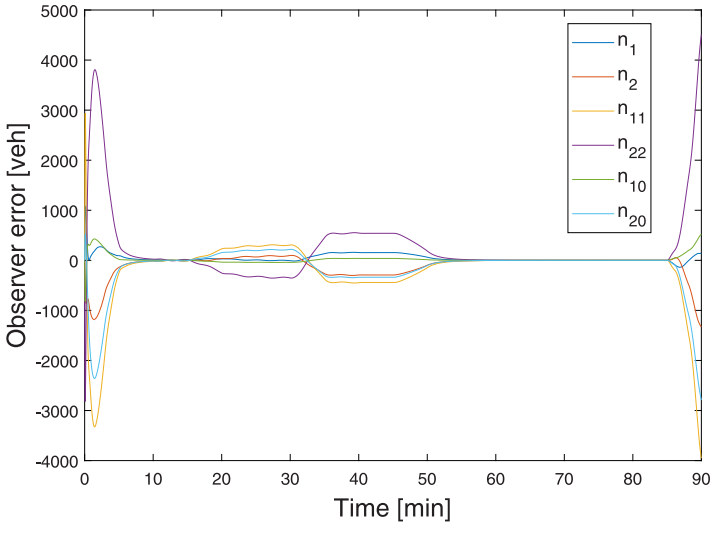

Fig. 9. Time evolution of the errors of the state estimator (observer) in case study (i). The errors are defined as $\widehat{\Delta n}(t) - (n(t) - n^*(t))$, where $\widehat{\Delta n}(t)$ is obtained from observer dynamics (12) and $n(t)$ is obtained from the nonlinear dynamics (4). The closed loop poles of the observer dynamics are placed arbitrarily at $[-8.8 - 8.6 - 8.2 - 8.3 - 8.4 - 8.7]$, and fast convergence of the estimated states to their true values is observed. Bounded observation errors between t=15 and t=55 [min] and after t=85 [min] are due to disturbance effects.

linear model: (i) Initial accumulations, (ii) best achievable performance gain γ, (iii) magnitude of disturbance (characterized by $\bar{d}$) during the operation of the network, and (iv) using the observed states rather than the actual states. It is clear that if the controllers are applied at the initial stages of congestion growth, the initial accumulations would remain close enough to their equilibrium values, resulting in further validity of the linearized model and thus a higher performance of the controllers. Moreover, a larger performance index γ could slow down the controller's reaction time, and thus deteriorate the controller's robust performance when applied to the nonlinear model. The disturbance magnitude and persistence influence the best achievable performance index γ, and have a direct impact on the performance of the controller. Large disturbances may push the system towards an unstable state, where the linear controllers could become ineffective. This explains the poor performance of the PI controller in this experiment, where a large performance index of $\gamma = 15.5$ has been obtained as the lowest admissible value from the criterion of Theorem 2.

Please cite this article as: R. Mohajerpoor, M. Saberi and H.L. Vu et al., H_∞ robust perimeter flow control in urban networks with partial information feedback, Transportation Research Part B, https://doi.org/10.1016/j.trb.2019.03.010

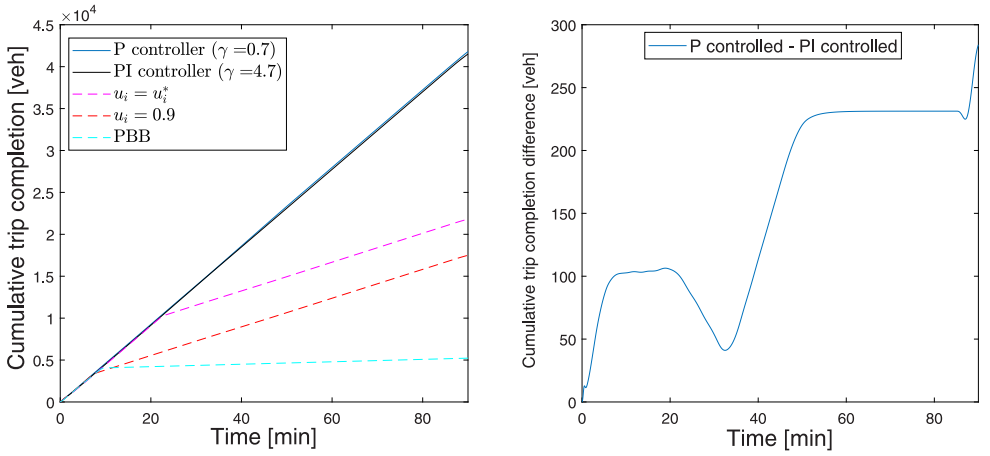

Fig. 10. Left: cumulative trip completions obtained from applying the following controllers in case study (i): 1. robust P controller with $\gamma = 0.7$, 2. robust PI controller with $\gamma = 4.7$, 3. SS control signals $u_k = u_k^*$ ($k \in \Omega_u$), 4. PBB controller (employing the actual states), and 5. fixed control $u_k = 0.9$. Right: the difference between the cumulative trip completions of the P and PI controllers.

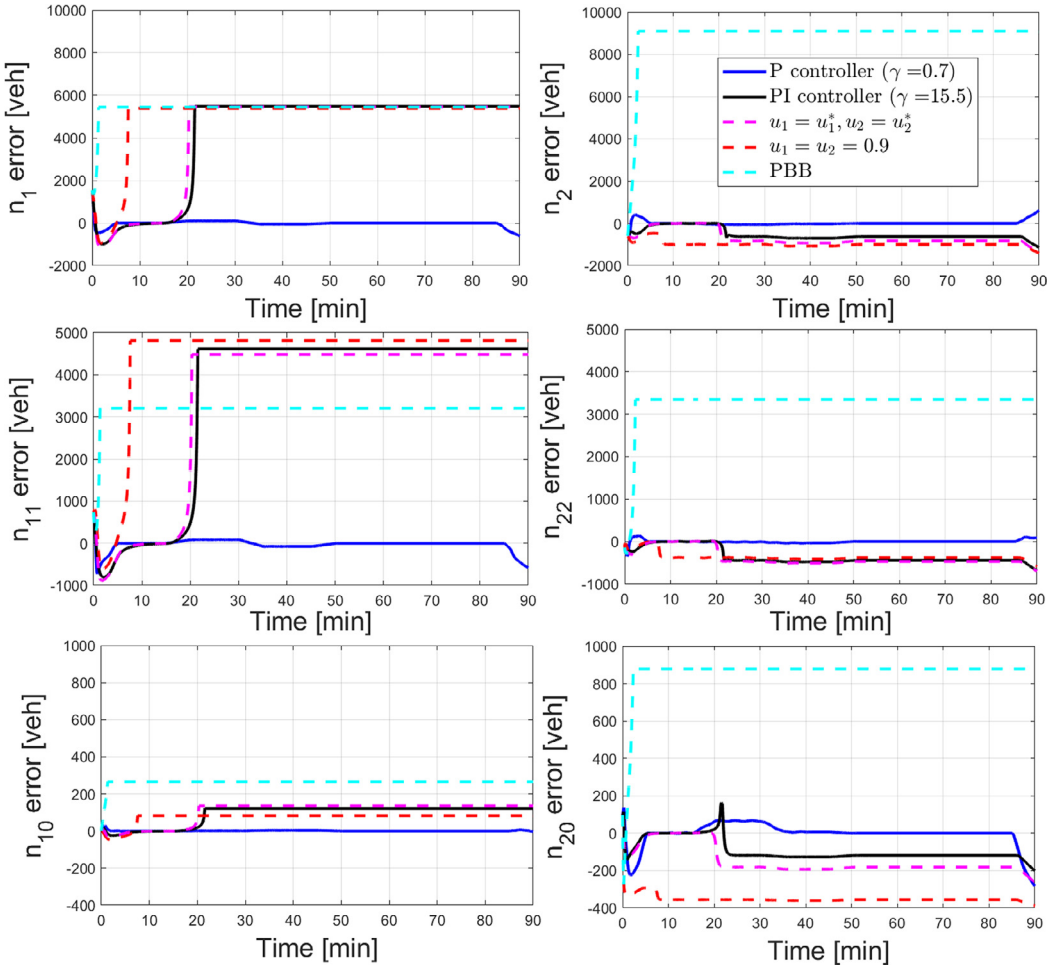

Fig. 11. Variations of accumulation errors ($n_i(t) - n_i^*$, $i \in \Omega_n$) of Regions 1 and 2 under various controllers applied to the nonlinear model in Case study (ii): 1. robust P controller with best achievable robust performance ($\gamma = 0.7$), 2. robust PI controller with best attainable robust performance ($\gamma = 15.5$), 3. PBB control algorithm (Algorithm 2), 4. the SS control signals ($u_k(t) = u_k^*$, $k \in \Omega_u$), and 5. fixed control $u_k = 0.9$. The PBB algorithm employs the actual states in examining Conditions I and II used in Algorithm 2.

Please cite this article as: R. Mohajerpoor, M. Saberi and H.L. Vu et al., H_∞ robust perimeter flow control in urban networks with partial information feedback, Transportation Research Part B, https://doi.org/10.1016/j.trb.2019.03.010

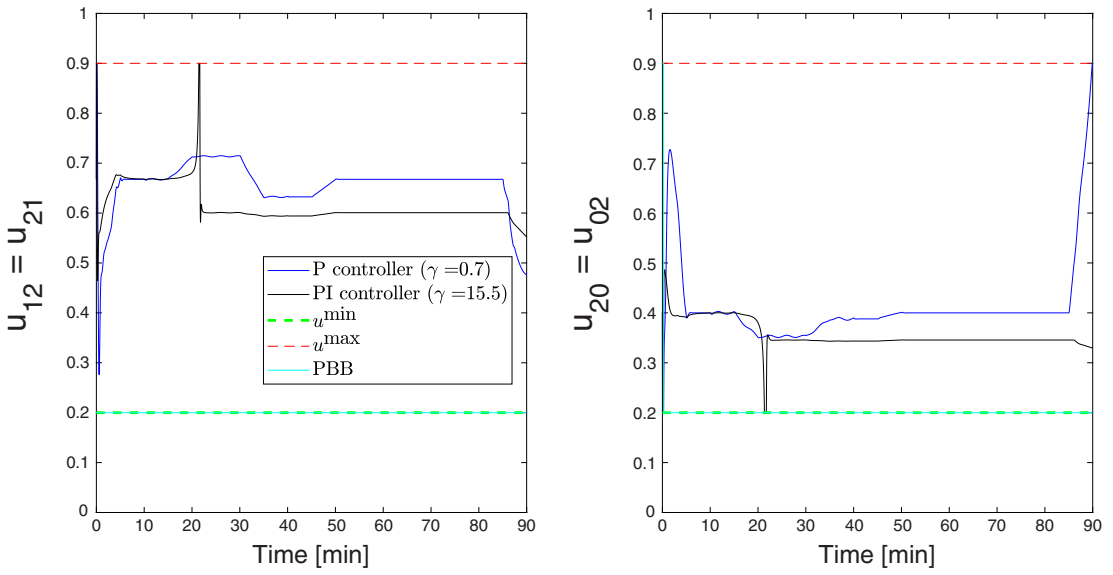

Fig. 12. Perimeter control signals with robust P, PI, and PBB control strategies applied to the nonlinear model for Case study (ii). The minimum and maximum admissible control values are shown by black and red dashed lines, respectively. Note that the PBB control signal in each sub-figure is the same as $u^{\min} = 0.2$. (For interpretation of the references to colour in this figure legend, the reader is referred to the web version of this article.)

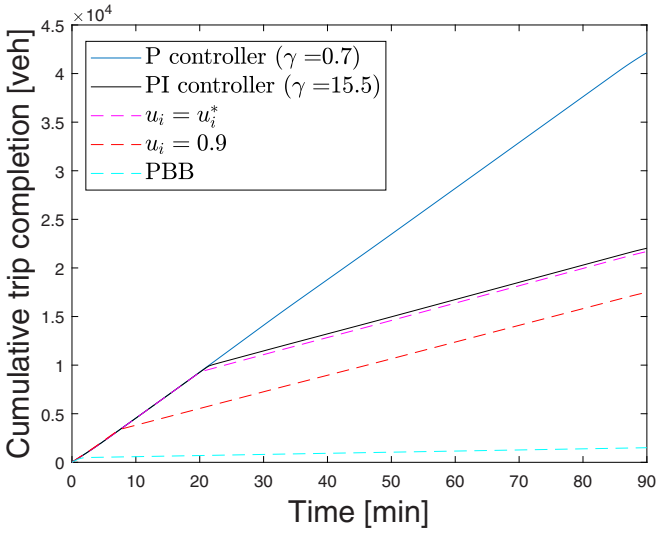

Fig. 13. Cumulative trip completions obtained from applying the following controllers in Case study (ii): 1. robust P controller with $\gamma = 0.7$, 2. robust PI controller with $\gamma = 15.5$ (the curve lies on top of the P controller scenario), 3. SS control signals $u_k = u_k^*$ ($k \in \Omega_u$), 4. PBB controller (employing the actual states), and 5. fixed control $u_k = 0.9$.

4.3. Case study (iii)

Since the main difference between Case studies (i) and (iii) is in the extent of the demand disturbances, the same SS solution and linearized matrices *A, B, C* are obtained. By applying Theorems 1 and 2, we obtain the control parameters resulting in the lowest admissible performance gains $\gamma = 0.7$ and $\gamma = 4.7$ for the robust P and PI controllers, respectively. Simulation results from applying control strategies (i)-(v), on the nonlinear model (4) are shown in Figs. 14–18.

Fig. 14 highlights that the proposed robust P and PI controllers maintain the accumulation of each region around their set-points. However, applying the SS control signals and the fixed control strategies result in gridlock of Regions 2 and 1, respectively. Furthermore, although the PBB algorithm employs the actual values of the states, it results in gridlock of both regions as in the previous case studies.

The reason for consistent fluctuations in the accumulation errors corresponding to the robust P and PI controllers is the consistent random demand fluctuations (see Fig. 4). The fluctuations also affect the observer errors as demonstrated in Fig. 15. As seen in the observer error dynamics (13), the demand disturbances directly influence the performance of the

Please cite this article as: R. Mohajerpoor, M. Saberi and H.L. Vu et al., H_∞ robust perimeter flow control in urban networks with partial information feedback, Transportation Research Part B, https://doi.org/10.1016/j.trb.2019.03.010

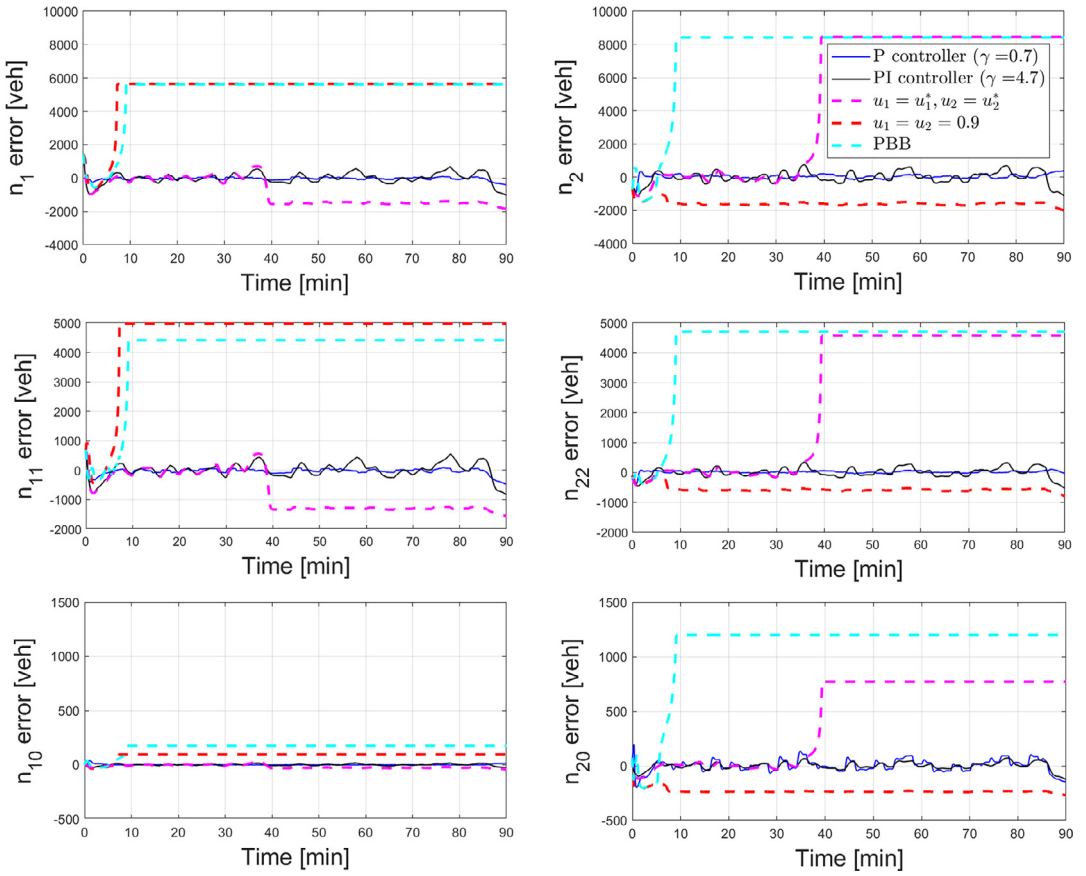

Fig. 14. Variations of accumulations errors ($n_i(t) - n_i^*,\ i \in \Omega_n$) under various controllers applied to the nonlinear model in Case study (iii): 1. robust P controller with best achievable robust performance ($\gamma = 0.7$), 2. robust PI controller with best attainable robust performance ($\gamma = 4.7$), 3. PBB control algorithm (Algorithm 2), 4. the SS control signals ($u_k(t) = u_k^*,\ k \in \Omega_u$), and 5. fixed control $u_k = 0.9$. The PBB algorithm employs the actual states in examining Conditions I and II used in Algorithm 2.

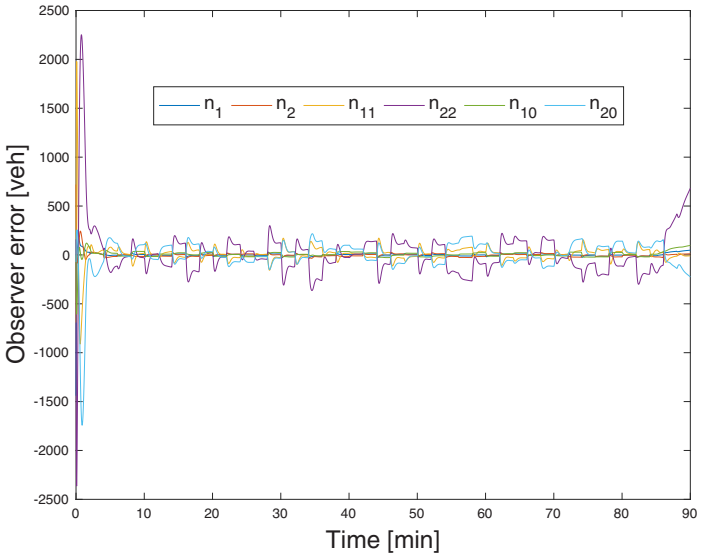

Fig. 15. Time evolution of the errors of the state estimator for Case study (iii). The errors are defined as $\widehat{\Delta n}(t) - (n(t) - n^*(t))$, where $\widehat{\Delta n}(t)$ is obtained from observer dynamics (12) and $n(t)$ is obtained from the nonlinear dynamics (4). The closed loop poles of the observer dynamics are placed arbitrarily at $[-8.8 - 8.6 - 8.2 - 8.3 - 8.4 - 8.7]$. The estimation errors remain bounded during the simulation and their magnitude is directly influenced by the norm of the disturbance effects.

Please cite this article as: R. Mohajerpoor, M. Saberi and H.L. Vu et al., H_∞ robust perimeter flow control in urban networks with partial information feedback, Transportation Research Part B, https://doi.org/10.1016/j.trb.2019.03.010

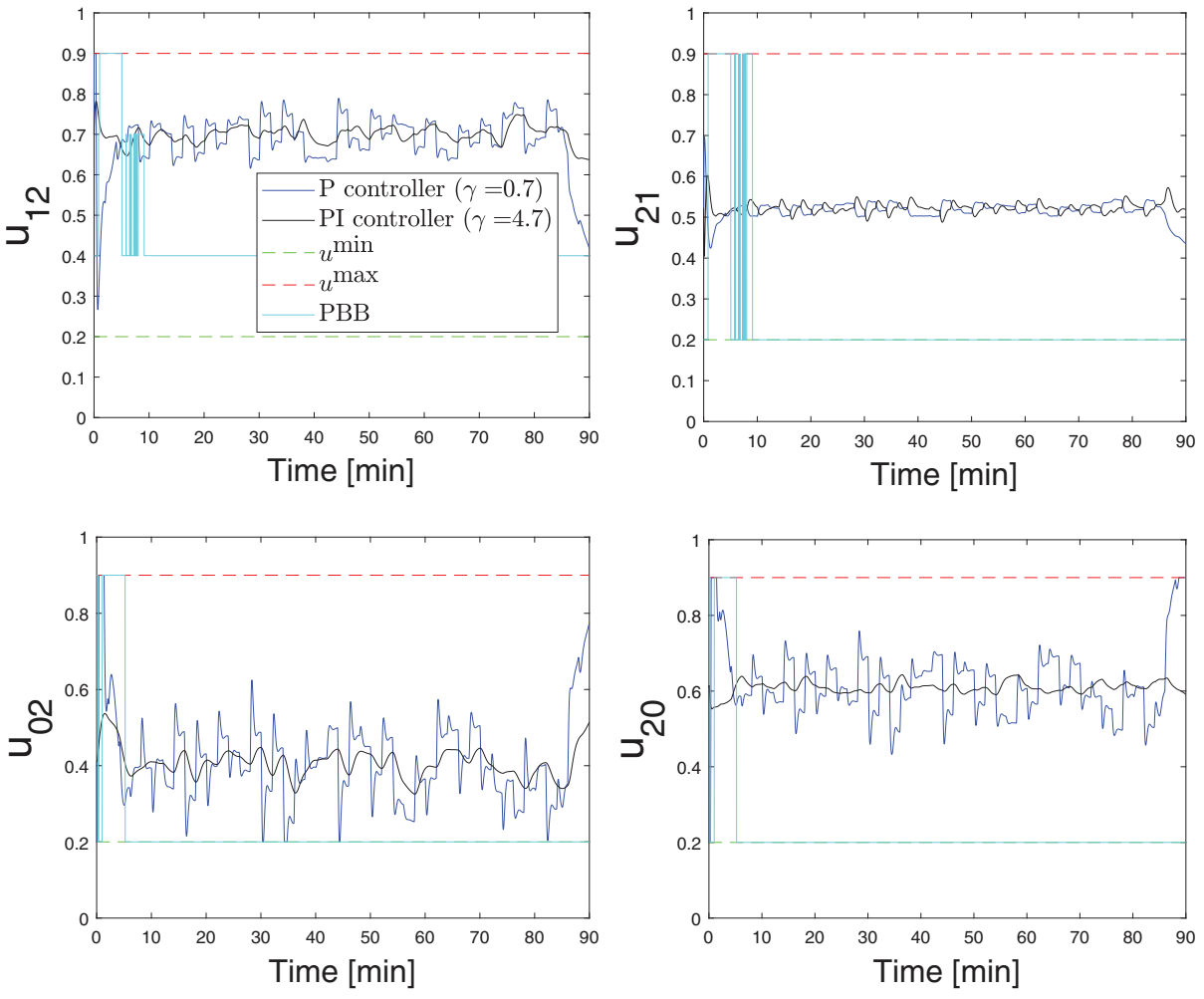

Fig. 16. Perimeter control signals with robust P and PI control strategies applied to the nonlinear model for Case study (iii). The minimum and maximum admissible control values are shown by black and red dashed lines, respectively. (For interpretation of the references to colour in this figure legend, the reader is referred to the web version of this article.)

observer, thus we see the growth of the observer errors whenever the demand disturbances grow in Figs. 9 and 15. Larger fluctuations are observed in the network with the PI controller, which is the result of larger best admissible H_∞ robust performance gain γ.

Moreover, it is shown in Fig. 16 that the control signals from both robust P and PI controllers remain within the allowable bounds, and Fig. 17 confirms that the offset between the control signals on each perimeter does not exceed the pre-specified threshold $\delta_i = 0.3$ when the P controller is applied. However, the difference occasionally exceeds the bounds when the PI controller is applied, which is due to the effects of nonlinearity of the model and poor robust performance of the controller (large γ). Nevertheless, due to the integral control actions, the PI controller returns smoother control signals in comparison with the P controller. In addition, Fig. 18 implies that the robust P and PI controllers exhibit the best performance, whereas the PBB algorithm shows the worst performance in minimizing the network's delay.

Finally, Table 2 reports the total trip completion of the network (also called the network throughput) at the end of demand period for Case studies (i)-(iii) when applying various control strategies. Overall, the proposed robust P and PI control strategies have been effective in improving the network's traffic congestion.

5. Summary and future works

This paper has developed robust, observer-based, H_∞ proportional and proportional-integral perimeter flow controllers. The traffic flow model is based on a multi-region accumulation-based MFD representation. The controllers can intake partial information from the network as feedback to relax the assumption of availability of the final destination of vehicles. The controllers that have been designed based on the Lyapunov approach guarantee (for the linearized system) the asymptotic

Please cite this article as: R. Mohajerpoor, M. Saberi and H.L. Vu et al., H_∞ robust perimeter flow control in urban networks with partial information feedback, Transportation Research Part B, https://doi.org/10.1016/j.trb.2019.03.010

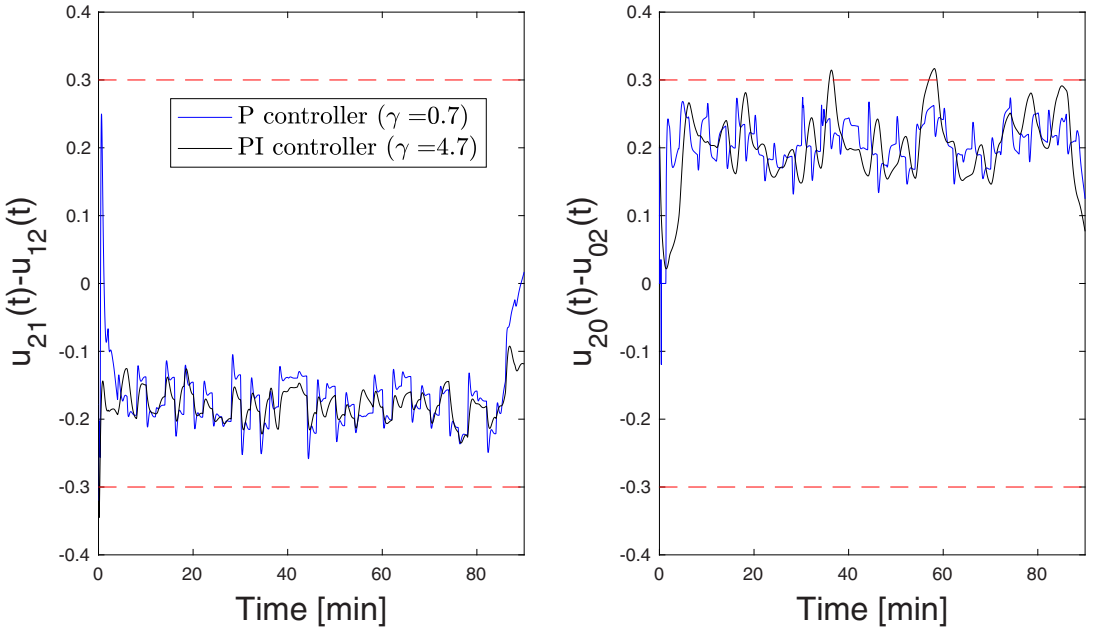

Fig. 17. The difference of the inbound and outbound perimeter control signals on perimeters 1 (left figure) and 2 (right figure) during the simulations of Case study (iii), when applying the robust P and PI controllers. The desired admissible bounds of the difference are highlighted by red dashed lines ($\delta_i = 0.3$). (For interpretation of the references to colour in this figure legend, the reader is referred to the web version of this article.)

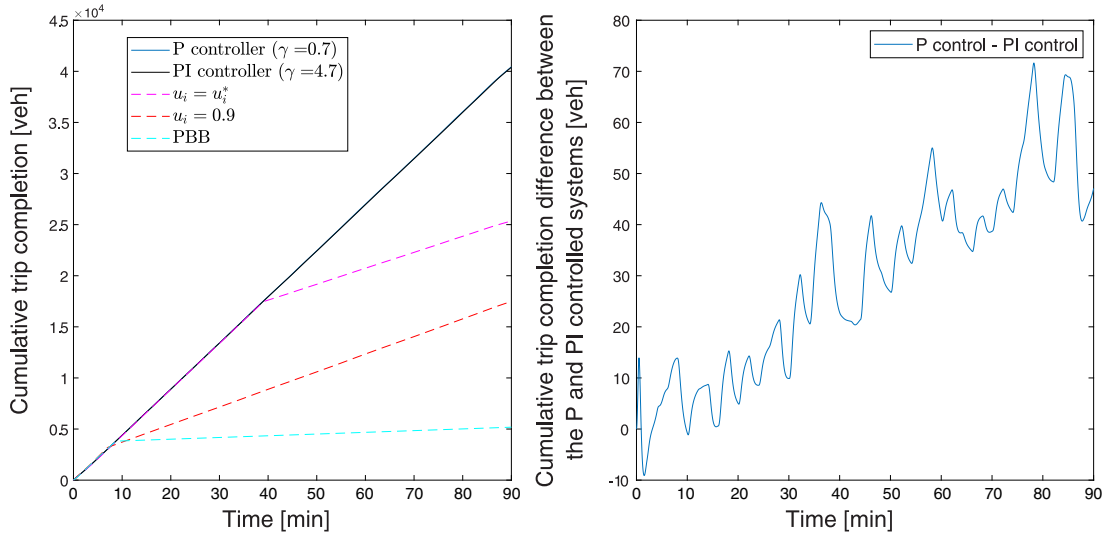

Fig. 18. Left: cumulative trip completions obtained from applying the following controllers in Case study (iii): 1. robust P controller with $\gamma = 0.7$, 2. robust PI controller with $\gamma = 4.7$ (the curve lies on top of the P controller scenario), 3. SS control signals $u_k = u_k^*$ ($k \in \Omega_u$), 4. PBB controller (employed estimated internal states), and 5. fixed control $u_k = 0.9$. Right: the difference between the cumulative trip completions of the P and PI controllers.

Table 2
Total cumulative network trip completion [veh] at the end of peak period of Case studies (i)-(iii) with various control strategies. The proportional controller has maximized the trip completion (highlighted in bold) and the PBB controller has had the worst performance (highlighted in italic) in each scenario.

Case study	P controller	PI controller	PBB controller	SS control	Fixed control
(i)	**41795**	41,511	*5226*	21,809	17500
(ii)	**42153**	22,024	*1503*	21,689	17497
(iii)	**40438**	40,391	*5180*	25,352	17478

Please cite this article as: R. Mohajerpoor, M. Saberi and H.L. Vu et al., H_∞ robust perimeter flow control in urban networks with partial information feedback, Transportation Research Part B, https://doi.org/10.1016/j.trb.2019.03.010

convergence of each region's accumulation to their desired value under zero fluctuations of demand. Furthermore, the controllers reject bounded fluctuations of the demand. The set-point states of the model are derived by solving an optimization problem. The control parameters are obtained off-line by solving a set of LMIs.

The controller design algorithms not only meet the crucial requirements on the boundedness of the perimeter control signals, but also guarantee a bounded difference between the inbound and outbound control signals on each perimeter. A nonlinear bang-bang type control algorithm has also been proposed for benchmarking aims. Implementation of the proposed robust control algorithms on the nonlinear model has emphasized their effectiveness in regulating the region accumulations, and their robust performance in accommodating large and persistent demand disturbances. It is realized that bounding the control signals and their differences on each perimeter can highly influence the performance of the designed dynamic controllers. Moreover, given that the P and PI controllers are designed for the linearized model, the H_∞ performance gain γ has a high impact on the stability and robust performance of actual nonlinear network. The PI controller has been more reactive and returns smoother control signals than the proportional controller. To add, the criterion to design the PI controller is numerically more efficient. However, the criterion to design the PI controller can be more conservative in the sense that it returns larger least admissible performance gain γ, which makes the controller slower in responding to demand perturbations, and thus the stability and robust performance of the actual network becomes more vulnerable.

In addition to the future works outlined in the paper, we will concentrate on a robust two-level control architecture, wherein a lower level controller will be added to adjust the signal timing of the gated intersections in an optimal manner (e.g. Mohajerpoor et al. (2019)). The lower level controller models and tackles the spillback and queues at the gated intersections Ramezani and Geroliminis (2015); Haddad (2017). The higher level controller will use a sampled-data framework to address the shortcomings due to cycle-by-cycle implementation of the controller. Moreover, the implementation of the proposed control algorithms on a microsimulation model can further examine their effectiveness in a more realistic situation. Coping with the uncertainties of MFDs and the hysteresis phenomena due to spatial density heterogeneity in the network are other crucial extensions of this research. Another sensible future extension is to consider a time-varying offset, $\delta(t)$, which takes into account more complex correlations between the control signals on a perimeter.

Acknowledgement

This research was partially supported by start-up fund of School of Civil Engineering, the University of Sydney; Monash University Faculties of Engineering and Science joint seed grant; and the Australian Road Research Board (ARRB) CEO innovation grant.

Appendix A. Detailed Expressions of Matrices A and B

The linearized state space matrices $A = [A_{ij}]_{\mathbf{s_n}\times\mathbf{s_n}}$ and $B = [B_{ij}]_{\mathbf{s_n}\times\mathbf{s_u}}$ of (8) are as follows:

- Non-zero elements of matrix A:

$$
\begin{aligned}
A_{11} &= -n_{11}^* F_{n1} - \bar{F}_{n1} u_{12}^* + n_{11}^* F_{n_1} u_{12}^*, & A_{33} &= -\tfrac{G_1(n_1^*)}{n_1^*},\\
A_{12} &= \bar{F}_{n_2} u_{21}^* - (n_{22}^* + n_{20}^*) F_{n_2} u_{21}^*, & A_{34} &= A_{36} = -\tfrac{G_2(n_2^*)}{n_2^*} u_{21}^*\\
A_{13} &= -\tfrac{G_1(n_1^*)}{n_1^*}(1 - u_{12}^*), & A_{41} &= (\bar{F}_{n_1} - F_{n_1} n_{11}^* + F_{n_1} n_{10}^*) u_{12}^*,\\
A_{14} &= A_{16} = -\tfrac{G_2(n_2^*)}{n_2^*} u_{21}^*, & A_{42} &= -F_{n_2} n_{22}^*,\\
A_{21} &= \bar{F}_{n_1} u_{12}^* - n_{11}^* F_{n_1} u_{12}^*, & A_{44} &= -\tfrac{G_2(n_2^*)}{n_2^*},\\
A_{22} &= -n_{22}^* F_{n_2} - \bar{F}_{n_2} u_{21}^* - n_{20}^* F_{n_2} u_{20}^* & A_{51} &= -n_{10}^* F_{n_1} u_{12}^*,\\
&\quad + (n_{22}^* + n_{20}^*) F_{n_2} u_{21}^*, & A_{55} &= -\tfrac{G_1(n_1^*)}{n_1^*} u_{12}^*,\\
A_{23} &= A_{43} = A_{45} = -\tfrac{G_1(n_1^*)}{n_1^*} u_{12}^*, & A_{61} &= n_{10}^* F_{n_1} u_{12}^*,\\
A_{24} &= -\tfrac{G_2(n_2^*)}{n_2^*}(1 - u_{21}^*), & A_{62} &= -n_{20}^* F_{n_2} u_{20}^*,\\
A_{26} &= \tfrac{G_2(n_2^*)}{n_2^*}(u_{21}^* - u_{20}^*), & A_{65} &= -A_{23},\\
A_{31} &= -F_{n_1} n_{11}^*, & A_{66} &= -\tfrac{G_2(n_2^*)}{n_2^*} u_{20}^*,\\
A_{32} &= (\bar{F}_{n_2} - F_{n_2} n_{20}^* - F_{n_2} n_{22}^*) u_{21}^*,
\end{aligned}
$$

where $\bar{F}_{n_i} = \frac{\partial G_i(n_i)}{\partial n_i}|_{n_i = n_i^*}$ and $F_{n_i} = \frac{\partial}{\partial n_i}[\frac{G_i(n_i)}{n_i}]|_{n_i = n_i^*}$, $i = \{1, 2\}$.

- Non-zero elements of matrix B:

$$
\begin{aligned}
B_{11} &= -(n_1^* - n_{11}^*)\tfrac{G_1(n_1^*)}{n_1^*}, & B_{32} &= (n_2^* - n_{22}^* - n_{20}^*)\tfrac{G_2(n_2^*)}{n_2^*},\\
B_{12} &= (n_2^* - n_{22}^* - n_{20}^*)\tfrac{G_2(n_2^*)}{n_2^*}, & B_{41} &= (n_1^* - n_{11}^* - n_{10}^*)\tfrac{G_1(n_1^*)}{n_1^*},\\
B_{21} &= -B_{11}, & B_{43} &= Q_{02}^*,\\
B_{22} &= -B_{12}, & B_{51} &= -\tfrac{n_{10}^*}{n_1^*} G_1(n_1^*),\\
B_{23} &= Q_0^*, & B_{61} &= -B_{51},\\
B_{24} &= -n_{20}^* \tfrac{G_2(n_2^*)}{n_2^*}, & B_{64} &= -\tfrac{n_{20}^*}{n_2^*} G_2(n_2^*).
\end{aligned}
$$

Appendix B. Proof of Theorem 1

Let us consider the following Lyapunov candidate function:

$$V(t) = x_P^T(t) P x_P, \tag{B.1}$$

where $P = \text{diag}(\text{P}_1, \text{P}_2)$ is symmetric and positive definite. We first prove the asymptotic stability of the closed-loop system when the disturbance $\Delta d(\cdot)$ is zero, and next its robust performance for nonzero disturbances. Assuming a null disturbance condition ($\Delta d(\cdot) \equiv 0$), and differentiating $V(t)$ along the solution of (14), we have

$$\dot{V}(t) = x_P^T(t) \Psi_P x_P(t), \tag{B.2}$$

where $\Psi_P = \begin{bmatrix} \text{He}(P_1 A + P_1 B K_P) & P_1 B K_P \\ * & \text{He}(P_2 A_c) \end{bmatrix}$.

If $\Psi_P \prec 0$, then according to the Lyapunov theorem Fridman (2014) the closed-loop dynamics (14) is globally asymptotically stable. Nevertheless, $\Psi_P \prec 0$ is not in the form of LMI due to the bilinear term $P_1 B K_P$. To resolve this issue, a congruence transformation using $\text{diag}(W_1, I_{s_n})$, where $W_1 = P_1^{-1}$, is applied. This results in Inequality (15), after recalling $Z_P = K_P W_1$ in (18).

To prove the robust performance in the presence of non-zero $\Delta d(t)$, we have

$$\dot{V}(t) + z^T(t) z(t) - \gamma^2 \Delta d^T(t) \Delta d(t) = \eta_P^T(t) \Psi_{P\infty} \eta_P(t),$$

where $\eta_P(t) = [x_P^T(t), \Delta d^T(t)]^T$, and

$$\Psi_{P\infty} = \begin{bmatrix} \text{He}(P_1 A + P_1 B K_P) + I_{s_n} & P_1 B K_P & P_1 \\ & \text{He}(P_2 A_c) & -P_2 \\ & * & -\gamma^2 I_{s_n} \end{bmatrix}.$$

Therefore, under zero initial conditions if in addition $\Psi_{P\infty} \prec 0$, the system meets the H_∞ performance criterion. After a congruence transformation using $\text{diag}(W_1, I_{s_n}, I_{s_n})$ and using the Schur complement lemma Boyd et al. (1994), it can be shown that $\Psi_{P\infty} \prec 0$ is equivalent to Inequality (19).

In addition, to fulfill the constraints on the control bounds (9), we have

$$-\Delta u_{(v)}^{\min} \le (K_P C_I)_{(v)} x_P(t) \le \Delta u_{(v)}^{\max},$$

where $C_I = [I_{s_n}, I_{s_n}]$. The above constraint can be reformulated as:

$$0 \le (K_P C_I)_{(v)} x_P(t) + \Delta u_v^{\min} \le \tilde{U}_v, \tag{B.3}$$

where $\tilde{U}_v \triangleq \Delta u_v^{\min} + \Delta u_v^{\max}$. By writing (B.3) in quadratic form, we have

$$x_P^T(t) (K_P C_I)_{(v)}^T (K_P C_I)_{(v)} x_P(t) + 2\Delta u_v^{\min} (K_P C_I)_{(v)} x_P(t) + \Delta u_v^{\min^2} \le \tilde{U}_v^2. \tag{B.4}$$

Furthermore, from $\dot{V}(t) + z^T(t) z(t) - \gamma^2 \Delta d^T(t) \Delta d(t) < 0$, we obtain

$$\dot{V}(t) - \gamma^2 \Delta d^T(t) \Delta d(t) \le 0.$$

Therefore, from (10)

$$V(t) = x_P^T(t) P x_P(t) \le \rho. \tag{B.5}$$

To add, from completing the squares (or Young's inequality), we have

$$2\Delta u_v^{\min} (K_P C_I)_{(v)} x_P(t) \le \Delta u_v^{\min^2} + \left((K_P C_I)_{(v)} x_P(t) \right)^2. \tag{B.6}$$

Noting that

$$x_P^T(t) (K_P C_I)_{(v)}^T (K_P C_I)_{(v)} x_P(t) = x_P^T(t) P^{0.5} P^{-0.5} (K_P C_I)_{(v)}^T (K_P C_I)_{(v)} P^{-0.5} P^{0.5} x_P(t),$$

it can be shown from (B.5) and (B.6) that (B.4) is equivalent to

$$2\rho P^{-0.5} (K_P C_I)_{(v)}^T (K_P C_I)_{(v)} P^{-0.5} - \tilde{u}_v I_{2s_n} \preceq 0. \tag{B.7}$$

Following the Schur complement lemma and a congruence transformation using $\text{diag}(W_1, I_{s_n}, 1)$, (B.7) can be written as LMI (16).

Hereafter, we show that Inequalities (17) guarantee the bounded difference of inbound and outbound control signals on each perimeter. From (3) and their SS form inequalities expressed in (O1), it can be shown that

$$-2\delta_i \le C_{u_i} \Delta u(t) \le 2\delta_i.$$

As such,

$$0 \le C_{u_i} K_P C_I x_P(t) + 2\delta_i \le 4\delta_i. \tag{B.8}$$

Please cite this article as: R. Mohajerpoor, M. Saberi and H.L. Vu et al., H_∞ robust perimeter flow control in urban networks with partial information feedback, Transportation Research Part B, https://doi.org/10.1016/j.trb.2019.03.010

Writing (B.8) in the quadratic form and completing the squares as in (B.6), we have

$$\|C_{u_i}K_PC_Ix_P(t)\|^2 - 2\delta_i \leq 0. \tag{B.9}$$

Now, from (B.5), Inequality (B.9) can be reformulated as

$$C_I^TK_P^TC_{u_i}^TC_{u_i}K_PC_I - \frac{4\delta_i^2}{\rho}P \preceq 0. \tag{B.10}$$

Applying the Schur complement lemma together with a congruence transformation using $\mathrm{diag}(W_1, I_{\mathbf{s_n}}, 1)$ on (B.10), result in Inequalities (17). This completes the proof of the theorem.

Appendix C. Proof of Theorem 2

We consider the following Lyapunov candidate function:

$$V(t) = x_{PI}^T(t)Px_{PI}(t), \tag{C.1}$$

where $P = \mathrm{diag}(\mathrm{P}_1, \mathrm{P}_2, \mathrm{P}_3)$ is symmetric and positive definite. Assuming a null disturbance condition ($\Delta d(\cdot) \equiv 0$), and differentiating $V(t)$ along the solution of (21), we have

$$\dot{V}(t) = x_{PI}^T(t)\Psi_{PI}x_{PI}(t), \tag{C.2}$$

where Ψ_{PI} is the left-hand-side of (22) and $Z_i = P_3K_i$ for $i = \{P, I\}$. As such, if $\Psi_{PI} \prec 0$, then according to the Lyapunov theorem the closed-loop dynamics (21) is globally asymptotically stable. In the presence of non-zero disturbance terms, one can write

$$\dot{V}(t) + z^T(t)z(t) - \gamma^2\Delta d^T(t)\Delta d(t) = \eta_{PI}^T(t)\Psi_{PI\infty}\eta_{PI}(t),$$

where $\eta_{PI}(t) = [x_{PI}^T(t), \Delta d^T(t)]^T$ and $\Psi_{PI\infty}$ is the left-hand-side of (25). Therefore, under zero initial conditions if in addition we have $\Psi_{PI\infty} \prec 0$, the system satisfies the H_∞ performance index.

Inequality (23) guarantees the boundedness of the control signals per condition (9), and (24) implies the constraints due to bounded difference of inbound and outbound control signals (3). Noting that $\Delta u(t) = \tilde{C}_{PI}x_{PI}$, the conditions can be proved following the same line as in the proof of Theorem 1 in Appendix B. Therefore, the statements of the theorem are proved.

Appendix D. The Heuristic Pseudo Bang Bang Network Control Algorithm

The criteria for switching the control signals is based on the congestion level of regions. The PBB algorithm minimizes (maximizes) the flow into the congested (uncongested) region. Accordingly, four possible situations may occur: Case I. the accumulations of both regions are less than their steady-state values, i.e. $n_i(t) \leq n_i^*$ ($i \in \{1, 2\}$); Case II. the accumulation of Region 2 is more than the SS accumulation (congested regime), but the accumulation of Region 1 is less than the SS value (uncongested regime), i.e. $n_1(t) \leq n_1^*$ and $n_2(t) > n_2^*$; Case III. the accumulation of Region 1 is more than the SS value, but the opposite holds for Region 2; and Case IV. both regions are in the congested regime. If both regions are congested (Case IV) at time $t > 0$ the algorithm considers the level of congestion as defined as $n_i(t)/n_i^*$ ($i = \{1, 2\}$) to evaluate which region is more congested.

One complication with this approach arises from condition (3), wherein the difference between the inbound and outbound control signals of Perimeter i is bounded by the threshold δ_i. To maximize or minimize the flow into Region 2, while satisfying (3), Conditions I and II below are defined. Condition I is satisfied when given $u_{12}(t) = u_{21}(t)$, the transfer flow from Region 2 to 1 is larger than that from Region 1 to 2. Likewise, the fulfillment of Condition II indicates a higher transfer flow from Region 2 to 0 for $u_{02}(t) = u_{20}(t)$.

Condition I:

$$\frac{n_{21}(t)}{n_2(t)}G_2(n_2(t)) - \frac{n_{12}(t) + n_{10}(t)}{n_1(t)}G_1(n_1(t)) > 0. \tag{D.1}$$

Condition II:

$$\frac{n_{20}(t)}{n_2(t)}G_2(n_2(t)) - Q_0(t) > 0. \tag{D.2}$$

Please cite this article as: R. Mohajerpoor, M. Saberi and H.L. Vu et al., H_∞ robust perimeter flow control in urban networks with partial information feedback, Transportation Research Part B, https://doi.org/10.1016/j.trb.2019.03.010

Algorithm 2 given below, summarizes our proposed PBB control scheme to regulate the accumulation of each region.

Algorithm 2 Pseudo bang-bang control algorithm to adjust the accumulation of each region at the desired value while maintaining Conditions (3).

Case	Control signals for Perimeter 1	Control signals for Perimeter 2
I. $n_i(t) \le n_i^*$, $i \in \{1,2\}$	$u_{12}(t) = u_{21}(t) = u_1^{\max}$	$u_{02}(t) = u_{20}(t) = u_2^{\max}$
II. $n_1(t) \le n_1^*$ and $n_2(t) > n_2^*$	• Condition I is satisfied: $u_{21}(t) = u_1^{\max}$; $u_{12}(t) = u_1^{\max} - \delta_1$ • Condition I is not satisfied: $u_{12}(t) = u_1^{\min}$; $u_{21}(t) = u_1^{\min} + \delta_1$	• Condition II is satisfied: $u_{20}(t) = u_2^{\max}$; $u_{02}(t) = u_2^{\max} - \delta_2$ • Condition II is not satisfied: $u_{02}(t) = u_2^{\min}$; $u_{20}(t) = u_2^{\min} + \delta_2$
III. $n_1(t) > n_1^*$ and $n_2(t) \le n_2^*$	• Condition I is satisfied: $u_{21}(t) = u_1^{\min}$; $u_{12}(t) = u_1^{\min} + \delta_1$ • Condition I is not satisfied: $u_{12}(t) = u_1^{\max}$; $u_{21}(t) = u_1^{\max} - \delta_1$	$u_{20}(t) = u_{02}(t) = u_2^{\max}$
IV. $n_1(t) > n_1^*$ and $n_2(t) > n_2^*$	**i.** $n_1(t)/n_1^{\mathrm{j}} \ge n_2(t)/n_2^{\mathrm{j}}$: • Condition I is satisfied: $u_{21}(t) = u_1^{\min}$; $u_{12}(t) = u_1^{\min} + \delta_1$ • Condition I is not satisfied: $u_{12}(t) = u_1^{\max}$; $u_{21}(t) = u_1^{\max} - \delta_1$ **ii.** $n_1(t)/n_1^{\mathrm{j}} < n_2(t)/n_2^{\mathrm{j}}$: • Condition I is satisfied: $u_{21}(t) = u_1^{\max}$; $u_{12}(t) = u_1^{\max} - \delta_1$ • Condition I is not satisfied: $u_{12}(t) = u_1^{\min}$; $u_{21}(t) = u_1^{\min} + \delta_1$	• Condition II is satisfied: $u_{20}(t) = u_2^{\max}$; $u_{02}(t) = u_2^{\max} - \delta_2$ • Condition II is not satisfied: $u_{02}(t) = u_2^{\min}$; $u_{20}(t) = u_2^{\min} + \delta_2$

Remark 8. Compared to the proposed P and PI control algorithms, the following limitations are intrinsically attached to the PBB control method: i) it requires knowledge of the internal states of the system; ii) it does not necessarily drive all the states to their SS values; iii) it may not be implementable in practice due to the high frequency of switching between the control levels. One suggestion to relax the first shortcoming could be using the estimated states $\hat{n}_{12}(t)$, $\hat{n}_{21}(t)$, $\hat{n}_{10}(t)$, and $\hat{n}_{20}(t)$ obtained from observer (12). However, this arrangement could itself deteriorate the network's outflow, and even result in gridlock of one or both regions (i.e. instability of the network).

Appendix E. Supplementary parameters of Section 4.1

- Characteristic matrices of the linearized model:

$$A = \begin{bmatrix} 0.56 & 2.08 & -1.89 & -3.35 & 0 & -3.35 \\ 3.66 & 0.63 & -4.40 & -3.07 & 0 & -0.56 \\ 4.22 & 2.08 & -6.28 & -3.35 & 0 & -3.35 \\ 3.56 & 2.38 & -4.40 & -6.43 & -4.40 & 0 \\ 0.11 & 0 & 0 & 0 & -4.40 & 0 \\ -0.11 & 0.33 & 0 & 0 & -4.40 & -3.91 \end{bmatrix}, \text{ and}$$

$$B = \begin{bmatrix} -3.6 & 10.54 & 0 & 0 \\ 3.6 & -10.54 & 5.04 & -2.37 \\ 0 & -10.54 & 0 & 0 \\ 3.09 & 0 & 2.16 & 0 \\ -0.51 & 0 & 0 & 0 \\ 0.51 & 0 & 0 & -2.37 \end{bmatrix} \times 10^3.$$

Please cite this article as: R. Mohajerpoor, M. Saberi and H.L. Vu et al., H_∞ robust perimeter flow control in urban networks with partial information feedback, Transportation Research Part B, https://doi.org/10.1016/j.trb.2019.03.010

- Observer gain:

$$L^T = \begin{bmatrix} 16.58 & 0.11 & 52.08 & -58.48 & -9.53 & 18.41 \\ -1.27 & 14.59 & -1.23 & -9.06 & 5.97 & 22.34 \end{bmatrix}.$$

- Control gain for the P controller:

$$K_P = \begin{bmatrix} 0.54 & 0.26 & -0.05 & -0.30 & -0.03 & -0.34 \\ 0.06 & -0.12 & -0.06 & -0.03 & -0.03 & -0.01 \\ -1.57 & -1.64 & 0.29 & 0.76 & -0.35 & 0.64 \\ -1.36 & -1.01 & 0.26 & 0.60 & -0.22 & 0.54 \end{bmatrix} \times 10^{-3}.$$

- Control gains for the PI controller:

$$K_P = \begin{bmatrix} 0.33 & -0.17 & 0.52 & 0.52 & 0.59 & 0.23 \\ -0.36 & -0.42 & 0.10 & 0.12 & 0.17 & 0.24 \\ 0.14 & -0.10 & 0.07 & 0.13 & 0.01 & 0.09 \\ 0.44 & -0.51 & 0.99 & 1.12 & 0.56 & 0.69 \end{bmatrix} \times 10^{-3},$$

$$K_I = \begin{bmatrix} -2.83 & -3.00 & 5.03 & 4.78 & 4.60 & 2.73 \\ -2.23 & 0.30 & 1.49 & 0.77 & 1.19 & 0.69 \\ -0.45 & -1.43 & 1.37 & 1.58 & 0.55 & 1.08 \\ -6.84 & -5.31 & 9.75 & 10.66 & 4.67 & 7.56 \end{bmatrix} \times 10^{-3}.$$

References

Aalipour, A., Kebriaei, H., Ramezani, M., 2018. Analytical optimal solution of perimeter traffic flow control based on mfd dynamics: a pontryagin's maximum principle approach. IEEE Trans. Intell. Transp. Syst. 1–11.
Aboudolas, K., Geroliminis, N., 2013. Perimeter and boundary flow control in multi-reservoir heterogeneous networks. Transp. Res. Part B 55, 265–281.
Amirgholy, M., Gonzales, E.J., 2016. Demand responsive transit systems with time-dependent demand: user equilibrium, system optimum, and management strategy. Transp. Res. Part B 92, 234–252.
Ampountolas, K., Zheng, N., Geroliminis, N., 2017. Macroscopic modelling and robust control of bi-modal multi-region urban road networks. Transp. Res. Part B 104, 616–637.
Apkarian, P., Noll, D., 2006. Nonsmooth h_∞ synthesis. Autom. Control, IEEE Trans. 51 (1), 71–86.
Boukal, Y., Darouach, M., Zasadzinski, M., Radhy, N., 2017. Robust h_∞ observer-based control of fractional-order systems with gain parametrization. IEEE Trans. Automat. Contr. 62 (11), 5710–5723.
Boyd, S., El Ghaoui, L., Feron, E., Balakrishnan, V., 1994. Linear matrix inequalities in system and control theory, 15. SIAM.
Brogan, W.L., 1982. Modern Control Theory. Pearson Education India.
Chiabaut, N., Küng, M., Menendez, M., Leclercq, L., 2018. Perimeter control as an alternative to dedicated bus lanes: a case study. Transp. Res. Rec. 2672 (20), 110–120.
Daganzo, C.F., 2007. Urban gridlock: macroscopic modeling and mitigation approaches. Transp. Res. Part B 41 (1), 49–62.
Doyle, J.C., Glover, K., Khargonekar, P.P., Francis, B.A., 1989. State-space solutions to standard h_2 and h_∞ control problems. IEEE Trans. Automat. Contr. 34 (8), 831–847. doi:10.1109/9.29425.
Fridman, E., 2014. Lyapunov-Based stability analysis. Introduction to Time-Delay Systems. Springer International Publishing.
Gahinet, P., Apkarian, P., 1994. A linear matrix inequality approach to h_∞ control. Int. J. Robust Nonlinear Control 4 (4), 421–448.
Geroliminis, N., Daganzo, C.F., 2008. Existence of urban-scale macroscopic fundamental diagrams: some experimental findings. Transp. Res. Part B 42 (9), 759–770.
Geroliminis, N., Haddad, J., Ramezani, M., 2013. Optimal perimeter control for two urban regions with macroscopic fundamental diagrams: a model predictive approach. IEEE Trans. Intell. Transp. Syst. 14 (1), 348–359.
Ghaoui, L.E., Oustry, F., AitRami, M., 1997. A cone complementarity linearization algorithm for static output-feedback and related problems. IEEE Trans. Automat. Contr. 42 (8), 1171–1176.
Gu, Z., Shafiei, S., Liu, Z., Saberi, M., 2018. Optimal distance- and time-dependent area-based pricing with the network fundamental diagram. Transp. Res. Part C 95, 1–28.
Haddad, J., 2017. Optimal perimeter control synthesis for two urban regions with aggregate boundary queue dynamics. Transp. Res. Part B 96, 1–25.
Haddad, J., Mirkin, B., 2016. Adaptive perimeter traffic control of urban road networks based on mfd model with time delays. Int. J. Robust Nonlinear Control 26 (6), 1267–1285.
Haddad, J., Mirkin, B., 2017. Coordinated distributed adaptive perimeter control for large-scale urban road networks. Transp. Res. Part C 77, 495–515.
Hamedmoghadam-Rafati, H., Steponavice, I., Ramezani, M., Saberi, M., 2017. A complex network analysis of macroscopic structure of taxi trips. 20th IFAC World Congress. IFAC-PapersOnLine 50 (1), 9432–9437.
Ji, Y., Geroliminis, N., 2012. On the spatial partitioning of urban transportation networks. Transp. Res. Part B 46 (10), 1639–1656.
Katebi, M.R., Moradi, M.H., 2001. Predictive pid controllers. IEE Proc.Control Theory Appl. 148 (6), 478–487.
Keyvan-Ekbatani, M., Kouvelas, A., Papamichail, I., Papageorgiou, M., 2012. Exploiting the fundamental diagram of urban networks for feedback-based gating. Transp. Res. Part B 46 (10), 1393–1403.
Keyvan-Ekbatani, M., Yildirimoglu, M., Geroliminis, N., Papageorgiou, M., 2015. Multiple concentric gating traffic control in large-scale urban networks. IEEE Trans. Intell. Transp. Syst. 16 (4), 2141–2154.
Khalil, H.K., Grizzle, J., 2002. Nonlinear systems, 3. Prentice hall Upper Saddle River.
Kouvelas, A., Saeedmanesh, M., Geroliminis, N., 2017. Enhancing model-based feedback perimeter control with data-driven online adaptive optimization. Transp. Res. Part B 96, 26–45.
Kutadinata, R., Moase, W., Manzie, C., Zhang, L., Garoni, T., 2016. Enhancing the performance of existing urban traffic light control through extremum-seeking. Transp. Res. Part C 62, 1–20.
Laval, J.A., Castrillón, F., 2015. Stochastic approximations for the macroscopic fundamental diagram of urban networks. Transp. Research Part B: Methodological 81, 904–916.
Leclercq, L., Chiabaut, N., Trinquier, B., 2014. Macroscopic fundamental diagrams: a cross-comparison of estimation methods. Transp. Res. Part B 62, 1–12.
Leclercq, L., Parzani, C., Knoop, V.L., Amourette, J., Hoogendoorn, S.P., 2015. Macroscopic traffic dynamics with heterogeneous route patterns. Transp. Res. Part C 59, 292–307.

Please cite this article as: R. Mohajerpoor, M. Saberi and H.L. Vu et al., H_∞ robust perimeter flow control in urban networks with partial information feedback, Transportation Research Part B, https://doi.org/10.1016/j.trb.2019.03.010

Lemarchand, A., Martinez Molina, J.J., Koenig, D., 2011. Smooth switching h_∞ pi controller for local traffic on-ramp metering, an lmi approach. 18th IFAC World Congress. IFAC Proceedings Volumes 44 (1), 13882–13887.
Liu, W., Geroliminis, N., 2017. Doubly dynamics for multi-modal networks with park-and-ride and adaptive pricing. Transp. Res. Part B 102, 162–179.
Loder, A., Ambühl, L., Menendez, M., Axhausen, K.W., 2017. Empirics of multi-modal traffic networks using the 3d macroscopic fundamental diagram. Transp. Res. Part C 82, 88–101.
Luk, J., Green, D., 2010. Balancing traffic density in a signalised network. Austroads.
Mahmassani, H.S., Saberi, M., Zockaie, A., 2013. Urban network gridlock: theory, characteristics, and dynamics. Transp. Res. Part C 36, 480–497.
Mariotte, G., Leclercq, L., Laval, J.A., 2017. Macroscopic urban dynamics: analytical and numerical comparisons of existing models. Transp. Res. Part B 101, 245–267.
Mohajerpoor, R., Abdi, H., Nahavandi, S., 2015. Minimal unknown-input functional observers for multi-input multi-output lti systems. J. Process Control 35, 143–153.
Mohajerpoor, R., Abdi, H., Nahavandi, S., 2015. A new algorithm to design minimal multi-functional observers for linear systems. Asian J. Control 18 (3), 842–857.
Mohajerpoor, R., Saberi, M., Ramezani, M., 2019. Analytical derivation of the optimal traffic signal timing: minimizing delay variability and spillback probability for undersaturated intersections. Transp. Res. Part B 119, 45–68.
Ramezani, M., Geroliminis, N., 2015. Queue profile estimation in congested urban networks with probe data. Comput.-Aided Civ. Infrastruct. Eng. 30 (6), 414–432.
Ramezani, M., Haddad, J., Geroliminis, N., 2015. Dynamics of heterogeneity in urban networks: aggregated traffic modeling and hierarchical control. Transp. Res. Part B 74, 1–19.
Ramezani, M., Nourinejad, M., 2018. Dynamic modeling and control of taxi services in large-scale urban networks: a macroscopic approach. Transp. Res. Part C 94, 203–219. ISTTT22
Saeedmanesh, M., Geroliminis, N., 2017. Dynamic clustering and propagation of congestion in heterogeneously congested urban traffic networks. Transp. Res. Part B 105, 193–211.
Wang, Y.J., Shieh, L.S., Sunkel, J., 1992. Observer-based robust h_∞ control laws for uncertain linear systems. J. Guidance Control Dyn. 15 (5), 1125–1133.
Yang, K., Zheng, N., Menendez, M., 2018. Multi-scale perimeter control approach in a connected-vehicle environment. ISTTT22. Transp. Res. Part C 94, 32–49.
Yildirimoglu, M., Ramezani, M., 2019. Demand management with limited cooperation among travellers: a doubly dynamic approach. Transp. Res. Part B.
Yildirimoglu, M., Ramezani, M., Geroliminis, N., 2015. Equilibrium analysis and route guidance in large-scale networks with mfd dynamics. Transp. Res. Part C 59, 404–420.
Yildirimoglu, M., Sirmatel, I.I., Geroliminis, N., 2018. Hierarchical control of heterogeneous large-scale urban road networks via path assignment and regional route guidance. Transp. Res. Part B 118, 106–123.
Zhong, R., Chen, C., Huang, Y., Sumalee, A., Lam, W., Xu, D., 2018. Robust perimeter control for two urban regions with macroscopic fundamental diagrams: a control-lyapunov function approach. TRB:ISTTT-22. Transp. Res. Part B 117, 687–707.
Zhong, R., Huang, Y., Chen, C., Lam, W., Xu, D., Sumalee, A., 2018. Boundary conditions and behavior of the macroscopic fundamental diagram based network traffic dynamics: a control systems perspective. Transp. Res. Part B 111, 327–355.

Please cite this article as: R. Mohajerpoor, M. Saberi and H.L. Vu et al., H_∞ robust perimeter flow control in urban networks with partial information feedback, Transportation Research Part B, https://doi.org/10.1016/j.trb.2019.03.010